The subcortical maternal complex protein Nlrp4f is involved in cytoplasmic lattice formation and organelle distribution

Dandan Qin[1, 2,*], Zheng Gao[1,3,*], Yi Xiao[1], Xiaoxin Zhang[1], Haixia Ma[1], Xingjiang Yu[1], Xiaoqing Nie[1,2], Na Fan[4], Xiaoqing Wang[1], Yingchun Ouyang[1], Qing-Yuan Sun[1], Zhaohong Yi[4], and Lei Li[1, 2, #]

[1]State Key Laboratory of Stem Cell and Reproductive Biology, Institute of Zoology, Chinese Academy of Sciences, Beijing, 100101, China. [2]University of Chinese Academy of Sciences, Beijing, 100049, China. [3]Reproductive Medicine Center of the Third Affiliated Hospital of Guangzhou Medical University, Guangzhou, 510150, China. [4]Key Laboratory of Urban Agriculture (North) of Ministry of Agriculture, College of Biological Science and Engineering, Beijing University of Agriculture, Beijing, 102206, China.

Keywords: SCMC, NLRP, organelle, cytoplasmic lattices, maternal effect gene, oocyte-to-embryo transition

* These authors contributed equally to this work

[#] To whom correspondence should be addressed: lil@ioz.ac.cn

Abstract

In mammalian oocytes and embryos, the subcortical maternal complex (SCMC) and cytoplasmic lattices (CPLs) are two closely related structures. Their detailed compositions and functions remain largely unclear. Here, we characterized Nlrp4f as a novel component associated with the SCMC and CPLs. Disruption of maternal Nlrp4f leads to decreased fecundity and delayed preimplantation development in the mouse. Lack of Nlrp4f affects organelle distribution in mouse oocytes and early embryos. Depletion of Nlrp4f disrupts CPL formation but does not affect the interactions of other SCMC proteins. Interestingly, the loss of Filia or Tle6, two other SCMC proteins, also disrupts CPL formation in mouse oocytes. Thus, the absence of CPLs and aberrant distribution of organelles in the oocytes disrupted the examined SCMC genes, including previously reported *Zbed3*, *Mater*, *Floped* and *Padi6*, indicate that the SCMC is required for CPL formation and organelle distribution. Consistent with the SCMC's role in CPL formation, the SCMC forms before CPLs during oogenesis. Together, our results suggest that SCMC protein Nlrp4f is involved in CPL formation and organelle distribution in mouse oocytes.

Introduction

Mammalian oocyte-to-embryo transition (OET) comprises numerous specific events including maternal RNAs clearance, organelles rearrangements, epigenetic reprogramming, and zygotic genome activation (Li et al., 2013; Lu et al., 2017). The low transcriptional activity during the OET indicates that maternal effect genes play essential roles in these events (Li et al., 2013; Li et al., 2010). Since the initial identification of the maternal-effect genes *Mater* and *Hsf1* (Christians et al., 2000; Tong et al., 2000), dozens of maternal effect genes have been reported to function in the oocyte-to-embryo transition (Condic, 2016; Li et al., 2010). Yet how the maternal effect genes regulate these events remains poorly understood.

We first described the SCMC as a 669-2000 KD molecular weight complex composed of several proteins encoded by maternal effect genes, including Floped, Mater, Tle6, Filia and Zbed3, and plausibly also Nlrp2 and Padi6 (Li et al., 2008; Lu et al., 2017). Based on their direct interactions and the roles in the stability of other SCMC proteins, the complex may include three core proteins (Floped, Mater, and Tle6) (Lu et al., 2017). Depletion of each SCMC core protein leads to the decreased expression level of other SCMC proteins and results in the arrested development at the 2-cell stage, suggesting an essential role of this complex in mouse early development and female fertility (Li et al., 2008; Tong et al., 2000; Yu et al., 2014). The SCMC is involved in multiple processes during the mouse OET, including cytoskeleton reorganization, organelle redistribution, and cell division (Gao et al., 2018; Lu et al., 2017; Tashiro et al., 2010; Yu et al., 2014). The SCMC genes and this complex may be conserved in other mammals, including humans (Bebbere et al., 2014; Lu et al., 2017; Zhu et al., 2015). Recently, mutations of several human genes encoding the SCMC proteins (Mater, Tle6, Filia, Nlrp2, and Padi6) were reported to be related to human reproductive disorders (Alazami et al., 2015; Docherty et al., 2015; Lu et al., 2017; Mu et al., 2019; Parry et al., 2011; Rezaei et al., 2016). However, how the SCMC regulates mammalian embryogenesis and fertility remains

largely unclear.

Several decades ago, CPLs, also known as cytoplasmic sheets, paracrystalline arrays, bilaminar lamellae or plaques, have been reported to specifically persist in mammalian oocytes and preimplantation embryos (Capco and Mcgaughey, 1986; Hadek, 1966; Weakley, 1966; Zamboni, 1970). CPL fibers are absent in primary oocytes, gradually appear as oocytes grow, become abundant in fully grown oocytes, and persist until the blastocyst stage (Gallicano et al., 1991; Wassarman and Josefowicz, 1978; Yurttas et al., 2008; Zamboni, 1970). CPLs undergoes large spatial rearrangements during fertilization, embryo compaction, and blastocyst formation (Capco and Mcgaughey, 1986; Gallicano et al., 1991). CPLs may be a specific structure of the cytoskeleton, including intermediate filaments or other unknown components (Capco et al., 1993; Gallicano et al., 1994). Padi6, also known as EPAD, is the first oocyte-specific protein identified to localize to CPLs in the mouse (Wright et al., 2003). Genetic depletion of *Padi6* results in the absence of CPLs, arrested development at the two-cell stage, and female infertile (Esposito et al., 2007). Padi6 is reported to associate with Mater and Floped (two SCMC proteins) that have been shown to localize to CPLs in mouse oocytes (Kim et al., 2010; Tashiro et al., 2010). CPLs are absent in oocytes from *Floped* and *Mater* null females (Kim et al., 2010; Tashiro et al., 2010). These results suggest a close relationship between the SCMC and CPLs.

NLRP subfamily proteins, containing an N-terminal pyrin domain (PYD), a NACHT nucleotide-binding domain and C-terminal leucine-rich repeats (LRRs), are well known for their roles in innate immunity where they participate in the assembly of inflammasomes (Martinon et al., 2007; Ratsimandresey et al., 2013; Zambetti et al., 2012). These subfamily proteins also play important roles in female reproduction in mammals (Kuchmiy et al., 2016; Mahadevan et al., 2017; Monk et al., 2017; Murdoch et al., 2006; Tong et al., 2000). *Nlrp4f* was initially identified as an oocyte-specific gene similar to *Mater*/*Nlrp5* in the mouse (Dade et al., 2004). Later, *Nlrp4f* was

identified as one of the downstream targets of FIGLA (Joshi et al., 2007). However, the physiological function of Nlrp4f remains unknown. Here, we characterized Nlrp4f as a novel component associated with the SCMC and CPLs. Genetic ablation of *Nlrp4f* shows that maternal Nlrp4f is required for mouse preimplantation development and female fertility. Furthermore, we investigate the relationship between the SCMC and CPLs using SCMC mutants, which indicate that the SCMC is involved in CPL formation.

Results

Identification of Nlrp4f as a novel component of the SCMC

CPLs are resistant to Triton X-100 extraction and are absent in *Mater* null oocytes (Gallicano et al., 1991; Kim et al., 2010). Using *Mater* null oocytes as a negative control, we extracted mouse oocytes with Triton X-100 to identify new components of CPLs (Materials and Methods). The insoluble and soluble fractions were separated by SDS-PAGE and stained with Coomassie brilliant blue staining (Fig. 1A). Two protein bands (band 1 and 2) in the insoluble fraction of *Mater*$^{+/+}$ and *Mater*$^{+/-}$ but not *Mater*$^{-/-}$ oocytes were analyzed by tandem mass spectrometry (Fig. 1A). We identified Mater with 45 peptides as the primary protein in band 1 and Nlrp4f with 33 peptides in the band 2 as a novel component associated with CPLs. To confirm the mass spectrometry results, we extracted normal mouse GV oocytes with Triton X-100, and the insoluble fraction was examined by Western blot for Nlrp4f and other known CPLs associated proteins including Mater, Floped, Zbed3. Similar to the other related proteins of CPLs, Nlrp4f was resistant to Triton X-100 extraction (Fig. 1B, 1C). These data suggest that Nlrp4f is a novel component associated with the CPLs.

Using mouse anti-Tle6 antibody to precipitate the lysates of mouse oocytes combined with mass spectrometry, we previously identified 23 potential SCMC proteins including Tle6, Mater, Floped, Filia and Zbed3 (Gao et al., 2018), as well as Nlrp4f with 14 peptides (Fig. S1). Immunostaining showed that Nlrp4f co-localized with the SCMC protein Mater in the subcortex and cytoplasm of mouse oocytes, especially after extraction (Fig. 1D). Co-immunoprecipitation (Co-IP) showed that both Tle6 and Floped antibodies specifically precipitated Nlrp4f, as well as Floped and Tle6, in normal mouse ovarian lysates (Fig. 1E). Similar to the decreased level of SCMC proteins in the oocytes disrupted with SCMC core protein Mater, Tle6 and Floped (Gao et al., 2018; Li et al., 2008; Yu et al., 2014), Nlrp4f was also decreased in these oocytes (Fig. 1F, 1G). These results identify Nlrp4f as a novel component of the SCMC in mouse oocytes.

Nlrp4f is specifically expressed in mouse oocytes and early embryos

Quantitative RT-PCR (qRT-PCR) showed that *Nlrp4f* mRNA was highly expressed in mouse ovaries (Fig. 2A). Compared with the fully-grown oocytes, *Nlrp4f* mRNA persisted at high levels in 1-cell stage embryos but decreased in 2-cell stage embryos (Fig. 2B). Western blots showed that Nlrp4f was primarily detected in mouse ovaries, but not in other tissues (Fig. 2C). In mouse oocyte and preimplantation embryos, Nlrp4f protein remained at high levels until the morula stage (Fig. 2D). Immunofluorescence showed that Nlrp4f protein was localized in the cytoplasm of oocytes and preimplantation embryos, and concentrated at their subcortex (Fig. 2E).These data suggest that *Nlrp4f* is an oocyte and embryo specific gene in the mouse.

Nlrp4f plays an important role in mouse female fertility

To investigate the role of Nlrp4f, we generated *Nlrp4f* knockout mice by targeting its exon 2 using CRISPR/Cas9 technology (Fig. S2A). DNA sequencing showed that a male founder was obtained with a mutation at *Nlrp4f* gene locus (Fig. S2A). This founder was used to establish the *Nlrp4f* mutant mouse line. *Nlrp4f*$^{-/-}$ mice grew into adults and appeared largely normal. The results of qRT-PCR revealed that *Nlrp4f* mRNA was absent in the oocytes from *Nlrp4f*$^{-/-}$ females (Fig. S2B). Western blots and immunostaining confirmed the successful ablation of Nlrp4f protein in the oocytes from *Nlrp4f*$^{-/-}$ females (Fig. S2C, S2D).

We then examined their fertility by mating. *Nlrp4f*$^{-/-}$ males exhibited normal fertility after mating for three months (Fig. 3A). However, compared with *Nlrp4f*$^{+/+}$ females, *Nlrp4f*$^{-/-}$ female mice produced fewer pups (Fig. 3A). We then performed hematoxylin and eosin staining for *Nlrp4f*$^{+/+}$ and *Nlrp4f*$^{-/-}$ ovaries. The results showed that primordial, growing and mature follicles, as well as corpora lutea (CL), were present in both *Nlrp4f*$^{+/+}$ and *Nlrp4f*$^{-/-}$ ovaries (Fig. 3B). We also examined the ratio of non-surrounded nucleolus (NSN)-type and surrounded nucleolus (SN)-type in fully grown oocytes from *Nlrp4f*$^{+/+}$ and *Nlrp4f*$^{-/-}$ ovaries. Compared with the controls, the ratio of NSN or SN oocytes from *Nlrp4f*$^{-/-}$ females did not significantly changed (Fig. S3A, S3B). Furthermore, similar numbers of MII oocytes were recovered from *Nlrp4f*$^{+/+}$ and *Nlrp4f*$^{-/-}$ females after superovulation with gonadotrophins (Fig. S4A, S4B). This suggests that Nlrp4f plays a role in female fertility but is not essential for mouse ovulation, and male fertility.

Nlrp4f is required for mouse preimplantation development

Next, we isolated preimplantation embryos from *Nlrp4f*$^{+/+}$ *and Nlrp4f*$^{-/-}$ females after mating with normal males. Similar numbers of 1- and 2-cell stage embryos were recovered from *Nlrp4f*$^{+/+}$ and *Nlrp4f*$^{-/-}$ females at E0.5 and E1.5 (Fig. 3C, 3D). The loss of maternal Nlrp4f had mininal effects on the total numbers of embryos at E2.5 and E3.5 (Fig. 3D). However, the majority of embryos from *Nlrp4f*$^{-/-}$ females displayed a delay in embryo compaction and blastocyst cavitation (Fig. 3C, 3D, S5). We also isolated 2-cell embryos from normal and *Nlrp4f*$^{-/-}$ females after the treatment with gonadotrophins and cultured these embryos *in vitro* for 60 hours. These cultured embryos also displayed similar developmental delays (Fig. 3E). Thus, Nlrp4f is also required for mouse preimplantation development.

Nlrp4f is involved in organelle distribution in oocytes and embryos

The distribution of organelles such as the ER and mitochondria is linked to early embryo and female fertility (Fernandes et al., 2012; Gao et al., 2018). Thus, we examined organelle distribution in zygotes from *Nlrp4f*$^{+/+}$ and *Nlrp4f*$^{-/-}$ females using ER-Tracker and Mito-Tracker to label the ER and mitochondria, respectively. In control zygotes from *Nlrp4f*$^{+/+}$ females, the ER and mitochondria concentrated around male and female pronucleus during interphase, and aggregated around the mitotic spindle following nuclear envelope broke down (NEBD) (Fig. 4A). However, in the zygotes from *Nlrp4f*$^{-/-}$ females, the ER and mitochondria concentrated around male and female pronucleus, and also aggregated in the subcortical region (Fig. 4A). Live imaging using Mito-Tracker confirmed that depletion of Nlrp4f led to the disorganized distribution of mitochondria in the zygote (Fig. 4B, Movie S1, Movie S2).

We also examined ER and mitochondria distribution in oocytes from *Nlrp4f*$^{+/+}$ and *Nlrp4f*$^{-/-}$ females. Here, the organelles radially distributed around the nucleus at GV, around the spindles after GVBD, and also around the spindles at MII (Fig. 4C). However, in *Nlrp4f*$^{-/-}$ oocytes, they localized both around the nucleus and cortical region at GV stage, concentrated to the subcortical region after GVBD, and were dispersed throughout the cytoplasm at MII stage (Fig. 4C). Live imaging confirmed that depletion of Nlrp4f resulted in the defects of mitochondria distribution during mouse oocyte maturation (Fig. 4D, Movie S3, Movie S4). These data suggest that Nlrp4f is involved in organelle distribution or redistribution during mouse oocyte maturation and zygote development.

Nlrp4f is required for CPL formation in mouse oocytes

Microtubules (MT) and acetylated tubulin have previously been involved in organelle redistribution during mouse oocyte maturation (Gao et al., 2018; Kan et al., 2011). Thus, we examined their patterns in *Nlrp4f*$^{-/-}$ oocytes by Western blots. This revealed a decrease in acetylated-α-tubulin in *Nlrp4f*$^{-/-}$ GV and MII oocytes (Fig. 5A). The treatment with the deacetylase inhibitor trichostatin A (TSA) significantly increased the level of acetylated-α-tubulin in both oocytes from *Nlrp4f*$^{+/+}$ and *Nlrp4f*$^{-/-}$ females (Fig. 5B, S6A). However, TSA treatment did not rescue the disorganized distribution of organelles in *Nlrp4f*$^{-/-}$ oocytes (Fig. 5C). Immunostaining showed that spindle MTs formed in both *Nlrp4f*$^{-/-}$ and control oocytes after GVBD, but the astral-like MTs were longer in *Nlrp4f*$^{-/-}$ oocytes than those in *Nlrp4f*$^{+/+}$ oocytes following GVBD (Fig. 5D). However, nocodazole treatment did not dramatically affect the subcortical distribution of organelles in 64% (30/47) *Nlrp4f*$^{-/-}$ oocytes after GVBD (Fig. 5E, S6B), suggesting that the lengthened microtubules may not be the predominant cause localizing the organelles to the subcortex in *Nlrp4f*$^{-/-}$ oocytes.

As CPLs may also be associated with organelle distribution in oocytes (Gao et al., 2018; Kan et al., 2011), we investigated CPLs in the ovaries of *Nlrp4f*$^{+/+}$ and *Nlrp4f*$^{-/-}$ using transmission electron microscope. As expected, CPLs were abundant in control oocytes of *Nlrp4f*$^{+/+}$ ovaries (Fig. 5F). However, CPLs were largely absent in the oocytes of *Nlrp4f*$^{-/-}$ ovaries (Fig. 5F), suggesting that Nlrp4f is required for CPL formation.

The SCMC is required for CPL formation and organelle distribtion

Although the SCMC core-protein Mater, Tle6, and Floped were necessary for the stability of Nlrp4f (Fig. 1F, 1G), depletion of Nlrp4f did not affect expression levels of other SCMC proteins including Mater, Tle6, Floped, and Zbed3 (Fig. S7A, S7B). Furthermore, depletion of Nlrp4f did not affect their interactions of these SCMC proteins (Fig. S7C). These results suggest that Nlrp4f is not a core component of the SCMC.

The absence of CPL formation in *Nlrp4f* null oocytes is reminiscent to oocytes depleted for Zbed3, which is also not the core component of the SCMC (Fig. 5F) (Gao et al., 2018). These results suggest that the integrity of the SCMC or any of the SCMC proteins is required for the formation of CPLs. To test this, we analyzed CPLs in the oocytes depleted with other SCMC proteins. We focused on Tle6, a core SCMC protein, and on Filia, another SCMC protein. Our results revealed that the CPLs were largely absent in *Tle6*$^{-/-}$ and *Filia*$^{-/-}$ oocytes (Fig. 6A and 6B). We also observed the aberrant distribution of organelles in *Filia*$^{-/-}$ oocytes (Fig. S8). Cosidering the absence of CPLs and the aberrant distribution of organelles in the oocytes disrupted for Nlrp4f, Filia and Tle6, as well as Zbed3, Mater, Floped and Padi6 (Fig.4, 5F, and Fig. S8) (Gao et al., 2018; Kan et al., 2011; Kim et al., 2010; Tashiro et al., 2010; Yurttas et al., 2008), we propose that the SCMC is required for CPL formation and organelle distribution in mouse oocytes.

The SCMC forms before CPL formation during mouse oogenesis

Although the CPLs were absent in *Nlrp4f* and *Zbed3* null oocytes, the SCMC was not affected (Fig. 5F, S7) (Gao et al., 2018), suggesting that the SCMC or at least its core complex, was the upstream regulator of CPL formation. To test this, we examined the expression of SCMC proteins in normal ovaries at postnatal day (PND) 1, 2, 3, 5, 10, 17, and 21. Although mRNA levels of the SCMC genes *Nlrp4f*, *Floped*, *Mater*, *Tle6* and *Zbed3* were highly expressed in the ovary when mice were born (Joshi et al., 2007; Li et al., 2008), these SCMC proteins were detected at low levels in the oocytes of normal mouse ovaries at this stage by immunostaining and Western blot (Fig. 6C, 6D). Importantly, these SCMC proteins were specifically co-precipitated by Tle6 antibody in normal ovarian lysates after PND 3 (Fig. 6E). CPLs were sporadically observed in the oocytes of ovaries at PND 5~10, but not observed in oocytes of ovaries at PND 3 (Wassarman and Josefowicz, 1978; Yurttas et al., 2008; Zamboni, 1970). Thus, our results suggest that the SCMC forms prior to CPLs in the oocytes of mouse ovaries, further supporting the idea that the SCMC is involved in CPL formation.

Discussion

CPLs were first discovered as an abundant structure in mammalian oocytes and early embryos (Gallicano et al., 1991; Hadek, 1966; Weakley, 1966; weakley, 1968; Zamboni, 1970). However, the role and composition of this structure remained mysterious. Recently, Padi6 was identified as an oocyte-embryo specific protein localized in the CPLs of mouse oocytes (Wright et al., 2003). Depletion of *Padi6* resulted in the absence of CPLs and arrested development at the 2-cell stage, suggesting the role of CPLs in development and female fertility (Esposito et al., 2007). More recently, the SCMC core proteins Mater and Floped were reported to localize to

CPLs and be required for CPL formation and 2-cell embryo development (Li et al., 2008; Tashiro et al., 2010; Tong et al., 2000). However, disruption of the associated SCMC proteins Zbed3, Nlrp4f, and Filia also results in the loss of CPLs, but the phenotypes are less severe for preimplantation development and female fecundity (Fig. 3, 5F) (Gao et al., 2018; Zheng and Dean, 2009). These results suggest that disruption of CPL formation is not the major cause of arrested development at the 2-cell stage and infertility in *Floped*, *Mater*, *Tle6,* and *Padi6* null females. Consistent with this, a recent report shows that CPL formation may not be related to the arrested 2-cell development in the mouse (Longo et al., 2018).

CPLs occupy large spaces of cytoplasm in mouse oocytes and early embryos (Capco and Mcgaughey, 1986; Gallicano et al., 1991; Zamboni, 1970). Some CPLs were observed to surround the organelles in mouse oocytes (Gao et al., 2018; Kan et al., 2011). These results suggest a role of CPLs in maintaining the localization of organelles in mouse oocytes. Consistent with this, the absence of CPLs is related to defects in organelle distribution in the oocytes with disruption of SCMC proteins Nlrp4f, Zbed3, Filia, Mater, Floped, Tle6, and Padi6 (Fig. 4) (Gao et al., 2018; Kan et al., 2011; Kim et al., 2010; Tashiro et al., 2010; Yurttas et al., 2008). Furthermore, CPLs contain intermediate filaments in mammalian oocytes and early embryos (Capco et al., 1993; Gallicano et al., 1994). The intermediate filaments directly or indirectly interact with other two cytoskeletons comprising microfilaments and microtubules, and regulate their dynamics of cytoskeletons in various cell types (Huber et al., 2015). Thus, CPLs may regulate microfilaments and microtubules in mouse oocytes and early embryos. Consistently, the absence of CPLs is related to the disorganized formation of microfilaments and microtubules in oocytes and embryos with disruption of the SCMC genes (Fig. 5) (Gao et al., 2018; Kan et al., 2011; Yu et al., 2014). Thus, CPLs may control organelle redistribution through the cytoskeletons in mouse oocytes and early embryos.

Three SCMC related proteins including Padi6, Floped, and Mater localized to CPLs of mouse oocytes (Tashiro et al., 2010; Wright et al., 2003). Disruption of all examined SCMC protein including Padi6, Mater, Floped, Tle6, Filia, Zbed3, and Nlrp4f lead to loss of CPLs in mouse oocytes (Fig. 5F, Fig. 6A, 6B) (Esposito et al., 2007; Gao et al., 2018; Kim et al., 2010; Tashiro et al., 2010). These results suggest that the SCMC is closely related to CPLs or they are the same structures in mouse oocytes (Kim et al., 2010; Tashiro et al., 2010). However, depletion of Zbed3 and Nlrp4f does not affect the stability of other SCMC proteins including Mater, Floped and Tle6, nor their interactions of these proteins (Fig. S7) (Gao et al., 2018), suggesting that the SCMC, or at least the SCMC core complex may be distinct to and involved in CPLs formation. Consistent with this, SCMC proteins are expressed and the complex can form before the CPLs during mouse oogenesis (Fig. 6C-E) (Wassarman and Josefowicz, 1978). How the SCMC regulates CPL formation remains unknown. One possibility is that all SCMC proteins control the CPL formation via a common regulatory factor or pathway. Consistent with this, CPLs is preserved by glutaraldehyde, but not other fixatives such as osmium tetroxide, formaldehyde, and other short-chain aldehydes (Weakley, 1966; weakley, 1968).

The molecular mass of the SCMC is larger than the total mass of the firstly identified four proteins (Floped, Mater, Tle6, and Filia), suggesting additional proteins in this complex (Li et al., 2008; Li et al., 2013; Lu et al., 2017). Padi6 may also be involved in the SCMC (Kim et al., 2010; Li et al., 2008). Recently, another maternal effect gene, Nlrp2, has been reported to be associated with the SCMC, based on the *in vitro* interactions of Nlrp2 and SCMC proteins, their localization and similar phenotypes (Mahadevan et al., 2017). We have recently characterized Zbed3 as a novel component of the SCMC in mouse oocytes and early embryos (Gao et al., 2018). The SCMC may be conserved in other mammals, including humans (Bebbere et al., 2014; Lu et al., 2017; Zhu et al., 2015). These studies have prompted us to

propose that the SCMC is a functional module in the mammalian oocyte-to-embryo transition (Lu et al., 2017). Here, we identified Nlrp4f as a novel protein of the SCMC, further supporting the notion of functional module of the SCMC. Mater/Nlrp5 is the first NLRP subfamily protein identified in the SCMC (Li et al., 2008; Tong et al., 2000). Recently, NLRP2 was reported to be associated with the SCMC (Kuchmiy et al., 2016; Mahadevan et al., 2017). Similar to the expression patterns of SCMC genes, the transcripts of many NLRP subfamily members, such as Nlrp14, Nlrp4a-4g, and Nlrp9a-9c, are specifically expressed in ovarian tissue, oocytes, and preimplantation embryos (Hamatani et al., 2004). Thus, some of other NLRP proteins may also function in oocyte and early embryos through the SCMC.

In summary, we have characterized Nlrp4f as a novel component of the SCMC in the mouse. The absence of CPLs is related to the disorganized distribution of organelles in oocytes with depletion of any SCMC genes, suggesting that the SCMC may function through organelle distribution probably by the CPLs in mouse oocytes and female fertility. Accumulating evidences suggest that the mutations of human SCMC genes are related to female reproductive disorders, including recurrent embryonic loss, molar pregnancies, and imprinting disorders (Amoushahi et al., 2019; Begemann et al., 2018; Lu et al., 2017; Mu et al., 2019; Nguyen et al., 2018; Wang et al., 2018). Further studies of phenotypes in Nlrp4f and other SCMC gene mutants and exploration of the relationships between the SCMC and its proteins, CPLs and oocyte quality will contribute to understanding of human OET and pathogenesis of reproductive diseases.

Materials and Methods

Mice maintenance, oocyte and embryo collection and culture

All animal maintenance and manipulations were performed according to the guidelines of the Animal Care and Use Committee of the Institute of Zoology, Chinese Academy of Sciences.

6-8 week-old normal and *Nlrp4f*$^{-/-}$ females were stimulated with 5 IU pregnant mare serum gonadotrophin (PMSG). After 46-48 hrs, oocytes were recovered by scraping the surface of the ovaries with a 26-gauge needle in M2 medium. MII oocytes were collected at 13-15 hrs after additional stimulation with 5 IU human chorionic gonadotrophin (hCG). Zygotes, two-cell embryos, morulae, and blastocysts from normal and *Nlrp4f*$^{-/-}$ mice were collected at 24 hrs, 48 hrs, 72 hrs, and 96 hrs after hCG stimulation, respectively.

For *in vitro* culture, two-cell embryos were collected from *Nlrp4f*$^{+/+}$ and *Nlrp4f*$^{-/-}$ females mated with normal fertile males. These two-cell embryos were cultured in KSOM (Millipore, MR-121-D) at 37°C in 5% CO_2. The development of embryos was examined every four hours and the developmental rates of the embryos were calculated.

Oocyte extraction and mass spectrometry

Equal amounts of oocytes (~500 GV oocytes) were collected from *Mater*$^{+/+}$, *Mater*$^{+/-}$ and *Mater*$^{-/-}$ mice and extracted by a buffer containing 100 mM NaCl, 3 mM $MgCl_2$, 300 mM sucrose, 10 mM PIPES (pH 6.8), 0.5% TritonX-100 and 1× Complete Protease Inhibitor Cocktail (Roche) for 30 mins at room temperature. After the extraction, the oocytes were manually picked up as the insoluble fraction. The remains contained the soluble components of oocytes in the buffer and were as the soluble fraction. These samples were separated by SDS-PAGE and stained by SimplyBlue™ SafeStain (Invitrogen, LC6060) according to the manufacturer's

protocol. The specific bands in *Mater*$^{+/+}$ (wild type, WT) and *Mater*$^{+/-}$, but not in *Mater*$^{-/-}$ oocytes, were collected for mass spectrometry (NanoLC-LTQ-Orbitrap XL, Thermo Finnigan, San Jose, CA).

Generation of *Nlrp4f* knockout mice by using CRISPR/Cas9

As previously reported, the T7 promoter was added to the Cas9 encoding region using pX330 as the template (Yang et al., 2013). Cas9 PCR products were *in vitro* transcribed using *mMESSAGE mMACHINE T7 ULTRA Kit* (Ambion, AM1345). The *Nlrp4f* sgRNAs were designed using the online CRISPR design tool (http://crispr.mit.edu/) and cloned into the pUC57-sgRNA expression vector. The sgRNA PCR templates were amplified for *in vitro* transcription with *MAXIscript SP6/T7 In Vitro Transcription Kit,* according to the manufacturer protocol (Ambion, AM1322). 50 ng/μl of Cas9 mRNA and 25 ng/μl of sgRNAs were mixed and injected into the cytoplasm of CD1 mouse zygotes. The surviving zygotes were transplanted into the oviducts of pseudopregnant females to produce the offspring. The offspring were genotyped by PCR with specific primers for *Nlrp4f*: Forward primer, 5'-CTGAGGTCCCAGCTTGTGTC-3'; Reverse primer, 5'-TTGGCCCTATGGTAGATGCG-3'.

Fertility assessment

For assessing the fertility of male mice, two months old *Nlrp4f*$^{+/+}$ females were mated with *Nlrp4f*$^{+/+}$ and *Nlrp4f*$^{-/-}$ male mice by 2:1 co-caging. For female mice fertility test, two months old *Nlrp4f*$^{+/+}$ and *Nlrp4f*$^{-/-}$ female mice were mated with normal fertile males by 2:1 co-caging. The number of pups per litter was recorded. The results were calculated after they were mated for three consecutive months.

The antibodies

Rabbit anti-Nlrp4f antibody was generated with a standard protocol of Abmart (Shanghai, China). In briefly, two peptides selected from Nlrp4f were expressed in *Escherichia coli* (*E. coli*) Rosetta and purified with Ni2+ affinity columns. The purified peptides were mixed and used to immunize rabbits four times. The serum (the antibody) from the immunized rabbits was purified with Protein A. Sequence of Nlrp4f peptide 1: LSNCSLSEQCWDYLSEVLRQNKTLSHLDISSNDLKDEGLKILCRSLILPYCVLESLCL SCCGITERGCQDLAEVLKNNQNLKYLHVSYNKLKDTGVMLLCDAIKHPNCHLKDLQ LEACEITDASNEELCYAFMQCETLQTLNLMGNAFEV; and sequence of Nlrp4f peptide 2: SKNIHHKLYQCLETLSGNAELQEQIDGMRLFSCLFEMEDEAFLVKAMNCMQQINFV AKNYSDFIVAAYCLKHCSTLKKLSFSTENVLNEGDQSYMEELLICWNNMCSVFVRS KDIQELRIKDTNFNEPAIRVLYESLKYPSFTLNKLVAN. Primary and secondary antibodies were used as in the Table S1.

Hematoxylin and eosin (HE) and immunofluorescent staining

The ovaries from two-month-old females at different ages were fixed in Bouin solution overnight at room temperature (for HE), or fixed with 4% paraformaldehyde (PFA) in PBS (phosphate-buffered solution) overnight at 4°C (for immunofluorescent staining), embedded in paraffin and sectioned. The sections were dewaxed, rehydrated, and stained with HE staining. Or for immunostaining, the rehydrated sections were treated for antigen retrieval and washed with PBS for three times. The sections were blocked with 5% BSA for 1 hour at room temperature and incubated with primary antibodies (Table S1) overnight at 4°C. After washing with PBS for three times, the sections were incubated with secondary antibodies (Table S1) and Hochest 33342 for 1 hour at room temperature and were mounted for imaging.

For whole mount staining of oocytes and early embryos, the isolated oocytes and embryos were fixed with 4% PFA including 0.5% Triton X-100 at room temperature for 30 mins. The immunostaining was performed with primary antibodies and secondary antibodies as described above.

For classification of NSN and SN in fully grown oocytes, the oocytes were fixed with 4% PFA, permeabilized with 0.5% Triton X-100, blocked with 5% normal donkey serum and stained DNA with Hochest 33342. According to their chromatin configuration in the nucleus, oocytes were classified into three groups, including nonsurrounded nucleolus (NSN) type with diffused chromatin, surrounded nucleolus (SN) type with a typical ring chromatin, and Middle type with the diffused and half-ring chromatin. The images were acquired with LSM780 (Zeiss).

Immunoblot and co-immunoprecipitation

For immunoblot, different tissues were collected from CD1 mice. Total proteins were extracted using RIPA lysis buffer containing 50 mM Tris-HCl (pH 7.5), 150 mM NaCl, 1% sodium deoxycholate, 1% Triton X-100, 0.1% SDS, 5 mM EDTA, 1 mM Na_3VO_4, 5~10 mM NaF and complete EDTA-free Protease Inhibitor Cocktail (Roche). The lysate was incubated on ice for 15 mins and centrifuged at 12,000 rpm for 15 mins at 4°C. The supernatant was quantified using a BCA reagent kit (Beyotime, P0012-1). For oocytes sample, equal amounts of oocytes (50-200) were collected. Then, proteins were separated by 8-15% SDS-PAGE and transferred onto PVDF membrane. The membrane was pre-treated with 5% defatted milk for 1 hour at room temperature and incubated with primary antibodies (Table S1) overnight at 4°C. After washing with PBST three times, the membrane was incubated with horseradish peroxidase (HRP)-conjugated secondary antibodies (Table S1) for 1 hour at room temperature. The signals were developed with SuperSignal West Pico Chemiluminescent Substrate (Thermo Fisher Scientific, #34080) and analyzed with Quantity One software (Bio-Rad Laboratories).

For co-immunoprecipitation, ovaries were isolated from CD1 female mice of different ages. Total proteins were extracted using immunoprecipitation (IP) lysis buffer containing 25 mM Tris-HCl (pH 7.5), 150 mM NaCl, 1 mM EDTA, 1% NP-40, 5% glycerol, 1 mM Na_3VO_4, 2 mM NaF and complete EDTA-free Protease Inhibitor Cocktail (Roche). The samples of GV oocytes were added BSA (final concentration: 1%) to protect proteins from degradation. After centrifugation (12,000 rpm for 15 mins at 4°C), the lysates were incubated with mouse anti-Tle6 antibody or normal mouse IgG at 4°C for 3-4 hrs before Protein A/G magnetic beads (Selleck, B23202) were added. Following an additional incubation for 3 hrs at 4°C, the beads were washed with IP lysis buffer for five times and eluted with 1x SDS loading buffer. The samples were separated by SDS-PAGE, and Western blot was performed with specific antibodies.

Quantitative real-time PCR

According to the manufacturer's protocols, mRNAs of different tissues were extracted using RNAzol reagent (Molecular Research Center, RN190) and mRNA of mouse eggs or embryos were isolated using Dynabeads® mRNA DIRECT™ Micro Kit (Life technologies, 61021). Complementary DNA (cDNA) was synthesized using PrimeScript™ RT Reagent Kit (Takara, RR037A). Quantitative RT-PCR was conducted with EvaGreen 2 × qPCR MasterMix (Applied Biological Materials, MasterMix-S). The expression of target genes was normalized with *Gapdh. Nlrp4f* forward primer, 5'-TCATCCAACACTTGCTCCAGC-3'; *Nlrp4f* reverse primer: 5'-AAAGATGCCATCTTGTCTTCAGG-3'.

Mitochondria and ER labeling

Before live-imaging, mouse oocytes and zygotes were cultured in M2 and KSOM medium, respectively, with MitoTracker® Red CMXRos (1:10000, Invitrogen, M7512) and ER-Tracker™ Blue-White DPX (1:5000, Invitrogen, E12353) at 37°C in 5% CO_2

for 60 mins. The pictures of live-imaging were captured by UltraVIEW-VoX (Perkin Elmer).

For drug treatment, *Nlrp4f*$^{+/+}$ and *Nlrp4f*$^{-/-}$ GV oocytes were cultured in M2 medium supplemented with 3-isobutyl-1-methylxanthine (IBMX, 100 μg/ml, Sigma, I7018), and with DMSO, Trichostatin A (TSA , Beyotime, S1893, 2 μg/ml, for 12 hrs) or Nocodazole (Sigma, M1404, 2.5 μg/ml, for 2 hrs) at 37°C in 5% CO_2. These arrested oocytes were washed with M2 medium for three times to release from IBMX inhibition, cultured to GVBD in M2 medium with DMSO, TSA or Nocodazole, and labeled with MitoTracker® Red CMXRos.

Transmission electron microscopy

Electron microscopy was performed as previously described (Gao et al., 2018). Briefly, the ovaries were isolated from two months old females and were fixed in a buffer containing 2.5% glutaraldehyde, 4% PFA, and 0.1 M Na-cacodylate for 24 hrs at 4°C. After gradient dehydration, the samples were embedded in LX112 resin and performed ultrathin sections. The pictures of oocytes from the ovarian sections were imaged with transmission electron microscopy (Jeol, JEM-1230).

Statistical analysis

All experiments were performed at least three times with different samples. All statistics were analyzed by the Student's t-test in GraphPad Prism5 software and presented as mean ± SEM. *P < 0.05 were considered as a significant difference.

Acknowledgment

We thank Lijuan Wang, Shiwen Li, Xili Zhu and Hua Qin (Institute of Zoology Chinese Academy of Science) for technical assistance and Dr. Jurrien Dean at the NIH in the USA, Dr. Marcel van Duin at the Ferring Pharmaceuticals, and Dr. Nicolas Plachta at Agency for Science, Technology & Research, Singapore for their critical review of the manuscript.

Competing interests

The authors declare no competing or financial interests.

Author contributions

D.Q. and Z.G. designed and performed the major experiments, analyzed the data, and wrote the original manuscript. Y.X., Y.O. established the *Nlrp4f* null transgenic mouse line. X.Z. obtained the electron microscope data. H.M. performed mass spectrometry experiments. X.Y., X.N., N.F., W.X. contributed to mouse maintenance and technical support. Q.S., Z.Y. analyzed the data. L.L. initiated and organized the study, analyzed the data, and wrote the manuscript. All authors commented on the manuscript.

Funding

The work was supported by the National Key R&D Program of China (2018YFC1004500), the National Natural Science Foundation of China (31930033, 31590832, 31771633), and the Strategic Collaborative Research Program of the Ferring Institute of Reproductive Medicine, Ferring Pharmaceuticals and Chinese Academy of Sciences (FIRMB180202).

Reference

Alazami, A. M., Awad, S. M., Coskun, S., Al-Hassan, S., Hijazi, H., Abdulwahab, F. M., Poizat, C. and Alkuraya, F. S. (2015). TLE6 mutation causes the earliest known human embryonic lethality. *Genome biology* **16**, 240.

Amoushahi, M., Sunde, L. and Lykke-Hartmann, K. (2019). The pivotal roles of the NOD-like receptors with a PYD domain, NLRPs, in oocytes and early embryo development. *Biol Reprod*.

Bebbere, D., Ariu, F., Bogliolo, L., Masala, L., Murrone, O., Fattorini, M., Falchi, L. and Ledda, S. (2014). Expression of maternally derived KHDC3, NLRP5, OOEP and TLE6 is associated with oocyte developmental competence in the ovine species. *Bmc Dev Biol* **14**.

Begemann, M., Rezwan, F. I., Beygo, J., Docherty, L. E., Kolarova, J., Schroeder, C., Buiting, K., Chokkalingam, K., Degenhardt, F., Wakeling, E. L., et al. (2018). Maternal variants in NLRP and other maternal effect proteins are associated with multilocus imprinting disturbance in offspring. *J Med Genet* **55**, 497-504.

Capco, D. G., Gallicano, G. I., McGaughey, R. W., Downing, K. H. and Larabell, C. A. (1993). Cytoskeletal sheets of mammalian eggs and embryos: a lattice-like network of intermediate filaments. *Cell Motil Cytoskeleton* **24**, 85-99.

Capco, D. G. and Mcgaughey, R. W. (1986). Cytoskeletal Reorganization during Early Mammalian Development - Analysis Using Embedment-Free Sections. *Dev Biol* **115**, 446-458.

Christians, E., Davis, A. A., Thomas, S. D. and Benjamin, I. J. (2000). Maternal effect of Hsf1 on reproductive success. *Nature* **407**, 693-694.

Condic, M. L. (2016). The Role of Maternal-Effect Genes in Mammalian Development: Are Mammalian Embryos Really an Exception? *Stem Cell Rev Rep* **12**, 276-284.

Dade, S., Callebaut, I., Paillisson, A., Bontoux, M., Dalbies-Tran, R. and Monget, P. (2004). In silico identification and structural features of six new genes similar to MATER specifically expressed in the oocyte. *Biochem Biophys Res Commun* **324**, 547-553.

Docherty, L. E., Rezwan, F. I., Poole, R. L., Turner, C. L., Kivuva, E., Maher, E. R., Smithson, S. F., Hamilton-Shield, J. P., Patalan, M., Gizewska, M., et al. (2015). Mutations in NLRP5 are associated with reproductive wastage and multilocus imprinting disorders in humans. *Nat Commun* **6**, 8086.

Esposito, G., Vitale, A. M., Leijten, F. P. J., Strik, A. M., Koonen-Reemst, A. M. C. B., Yurttas, P., Robben, T. J. A. A., Coonrod, S. and Gossen, J. A. (2007). Peptidylarginine deiminase (PAD) 6 is essential for oocyte cytoskeletal sheet formation and female fertility. *Molecular and Cellular Endocrinology* **273**, 25-31.

Fernandes, R., Tsuda, C., Perumalsamy, A. L., Naranian, T., Chong, J., Acton, B. M., Tong, Z. B., Nelson, L. M. and Jurisicova, A. (2012). NLRP5 mediates mitochondrial function in mouse oocytes and embryos. *Biol Reprod* **86**, 138, 131-110.

Gallicano, G. I., Larabell, C. A., Mcgaughey, R. W. and Capco, D. G. (1994). Novel Cytoskeletal Elements in Mammalian Eggs Are Composed of a Unique Arrangement of Intermediate Filaments. *Mech Develop* **45**, 211-226.

Gallicano, G. I., Mcgaughey, R. W. and Capco, D. G. (1991). Cytoskeleton of the Mouse Egg and Embryo - Reorganization of Planar Elements. *Cell Motil Cytoskeleton* **18**, 143-154.

Gao, Z., Zhang, X., Yu, X., Qin, D., Xiao, Y., Yu, Y., Xiang, Y., Nie, X., Lu, X., Liu, W., et al. (2018). Zbed3 participates in the subcortical maternal complex and regulates the distribution of organelles. *Journal of molecular cell biology* **10**, 74-88.

Hadek, R. (1966). Cytoplasmic whorls in the golden hamster oocyte. *J Cell Sci* **1**, 281-282.

Huber, F., Boire, A., Lopez, M. P. and Koenderink, G. H. (2015). Cytoskeletal crosstalk: when three different personalities team up. *Current Opinion in Cell Biology* **32**, 39-47.

Joshi, S., Davies, H., Sims, L. P., Levy, S. E. and Dean, J. (2007). Ovarian gene expression in the absence of FIGLA, an oocyte-specific transcription factor. *Bmc Dev Biol* **7**.

Kan, R., Yurttas, P., Kim, B., Jin, M., Wo, L., Lee, B., Gosden, R. and Coonrod, S. A. (2011). Regulation of mouse oocyte microtubule and organelle dynamics by PADI6 and the cytoplasmic lattices. *Dev Biol* **350**, 311-322.

Kim, B., Kan, R., Anguish, L., Nelson, L. M. and Coonrod, S. A. (2010). Potential role for MATER in cytoplasmic lattice formation in murine oocytes. *PLoS One* **5**, e12587.

Kuchmiy, A. A., D'Hont, J., Hochepied, T. and Lamkanfi, M. (2016). NLRP2 controls age-associated maternal fertility. *J Exp Med* **213**, 2851-2860.

Li, L., Baibakov, B. and Dean, J. (2008). A subcortical maternal complex essential for preimplantation mouse embryogenesis. *Dev Cell* **15**, 416-425.

Li, L., Lu, X. and Dean, J. (2013). The maternal to zygotic transition in mammals. *Mol Aspects*

Med **34**, 919-938.

Li, L., Zheng, P. and Dean, J. (2010). Maternal control of early mouse development. *Development* **137**, 859-870.

Longo, M., Boiani, M., Redi, C. and Monti, M. (2018). Cytoplasmic lattices are not linked to mouse 2-cell embryos developmental arrest. *European journal of histochemistry : EJH* **62**.

Lu, X., Gao, Z., Qin, D. and Li, L. (2017). A Maternal Functional Module in the Mammalian Oocyte-To-Embryo Transition. *Trends in molecular medicine* **23**, 1014-1023.

Mahadevan, S., Sathappan, V., Utama, B., Lorenzo, I., Kaskar, K. and Van den Veyver, I. B. (2017). Maternally expressed NLRP2 links the subcortical maternal complex (SCMC) to fertility, embryogenesis and epigenetic reprogramming. *Scientific reports* **7**, 44667.

Martinon, F., Gaide, O., Petrilli, V., Mayor, A. and Tschopp, J. (2007). NALP inflammasomes: a central role in innate immunity. *Seminars in immunopathology* **29**, 213-229.

Monk, D., Sanchez-Delgado, M. and Fisher, R. (2017). NLRPs, the subcortical maternal complex and genomic imprinting. *Reproduction* **154**, R161-R170.

Mu, J., Wang, W., Chen, B., Wu, L., Li, B., Mao, X., Zhang, Z., Fu, J., Kuang, Y., Sun, X., et al. (2019). Mutations in NLRP2 and NLRP5 cause female infertility characterised by early embryonic arrest. *J Med Genet* **56**, 471-480.

Murdoch, S., Djuric, U., Mazhar, B., Seoud, M., Khan, R., Kuick, R., Bagga, R., Kircheisen, R., Ao, A., Ratti, B., et al. (2006). Mutations in NALP7 cause recurrent hydatidiform moles and reproductive wastage in humans. *Nat Genet* **38**, 300-302.

Nguyen, N. M. P., Khawajkie, Y., Mechtouf, N., Rezaei, M., Breguet, M., Kurvinen, E., Jagadeesh, S., Solmaz, A. E., Aguinaga, M., Hemida, R., et al. (2018). The genetics of recurrent hydatidiform moles: new insights and lessons from a comprehensive analysis of 113 patients. *Modern pathology : an official journal of the United States and Canadian Academy of Pathology, Inc* **31**, 1116-1130.

Parry, D. A., Logan, C. V., Hayward, B. E., Shires, M., Landolsi, H., Diggle, C., Carr, I., Rittore, C., Touitou, I., Philibert, L., et al. (2011). Mutations Causing Familial Biparental Hydatidiform Mole Implicate C6orf221 as a Possible Regulator of Genomic Imprinting in the Human Oocyte. *Am J Hum Genet* **89**, 451-458.

Ratsimandresey, R. A., Dorfleutner, A. and Stehlik, C. (2013). An Update on PYRIN

Domain-Containing Pattern Recognition Receptors: From Immunity to Pathology. *Frontiers in immunology* **4**, 440.

Rezaei, M., Nguyen, N. M., Foroughinia, L., Dash, P., Ahmadpour, F., Verma, I. C., Slim, R. and Fardaei, M. (2016). Two novel mutations in the KHDC3L gene in Asian patients with recurrent hydatidiform mole. *Human genome variation* **3**, 16027.

Tashiro, F., Kanai-Azuma, M., Miyazaki, S., Kato, M., Tanaka, T., Toyoda, S., Yamato, E., Kawakami, H., Miyazaki, T. and Miyazaki, J. (2010). Maternal-effect gene Ces5/Ooep/Moep19/Floped is essential for oocyte cytoplasmic lattice formation and embryonic development at the maternal-zygotic stage transition. *Genes Cells* **15**, 813-828.

Tong, Z. B., Gold, L., Pfeifer, K. E., Dorward, H., Lee, E., Bondy, C. A., Dean, J. and Nelson, L. M. (2000). Mater, a maternal effect gene required for early embryonic development in mice. *Nat Genet* **26**, 267-268.

Wang, X. Q., Song, D., Mykytenko, D., Kuang, Y. P., Lv, Q. F., Li, B., Chen, B. B., Mao, X. Y., Xu, Y., Zukin, V., et al. (2018). Novel mutations in genes encoding subcortical maternal complex proteins may cause human embryonic developmental arrest. *Reproductive Biomedicine Online* **36**, 698-704.

Wassarman, P. M. and Josefowicz, W. J. (1978). Oocyte development in the mouse: an ultrastructural comparison of oocytes isolated at various stages of growth and meiotic competence. *Journal of morphology* **156**, 209-235.

Weakley, B. S. (1966). Electron microscopy of the oocyte and granulosa cells in the developing ovarian follicles of the golden hamster (Mesocricetus auratus). *Journal of anatomy* **100**, 503-534.

Weakley, B. S. (1968). Comparison of cytoplasmic lamellae and membranous elements in the oocytes of five mammalian species. *Z Zellforsch Mikrosk Anat* **85**, 109-123.

Wright, P. W., Bolling, L. C., Calvert, M. E., Sarmento, O. F., Berkeley, E. V., Shea, M. C., Hao, Z., Jayes, F. C., Bush, L. A., Shetty, J., et al. (2003). ePAD, an oocyte and early embryo-abundant peptidylarginine deiminase-like protein that localizes to egg cytoplasmic sheets. *Dev Biol* **256**, 73-88.

Yang, H., Wang, H., Shivalila, C. S., Cheng, A. W., Shi, L. and Jaenisch, R. (2013). One-step generation of mice carrying reporter and conditional alleles by CRISPR/Cas-mediated

genome engineering. *Cell* **154**, 1370-1379.

Yu, X. J., Yi, Z., Gao, Z., Qin, D., Zhai, Y., Chen, X., Ou-Yang, Y., Wang, Z. B., Zheng, P., Zhu, M. S., et al. (2014). The subcortical maternal complex controls symmetric division of mouse zygotes by regulating F-actin dynamics. *Nat Commun* **5**, 4887.

Yurttas, P., Vitale, A. M., Fitzhenry, R. J., Cohen-Gould, L., Wu, W., Gossen, J. A. and Coonrod, S. A. (2008). Role for PADI6 and the cytoplasmic lattices in ribosomal storage in oocytes and translational control in the early mouse embryo. *Development* **135**, 2627-2636.

Zambetti, L. P., Laudisi, F., Licandro, G., Ricciardi-Castagnoli, P. and Mortellaro, A. (2012). The rhapsody of NLRPs: master players of inflammation...and a lot more. *Immunologic research* **53**, 78-90.

Zamboni, L. (1970). Ultrastructure of mammalian oocytes and ova. *Biol Reprod* **2**, Suppl 2:44-63.

Zheng, P. and Dean, J. (2009). Role of Filia, a maternal effect gene, in maintaining euploidy during cleavage-stage mouse embryogenesis. *Proc Natl Acad Sci U S A* **106**, 7473-7478.

Zhu, K., Yan, L., Zhang, X., Lu, X., Wang, T., Yan, J., Liu, X., Qiao, J. and Li, L. (2015). Identification of a human subcortical maternal complex. *Mol Hum Reprod* **21**, 320-329.

Figures

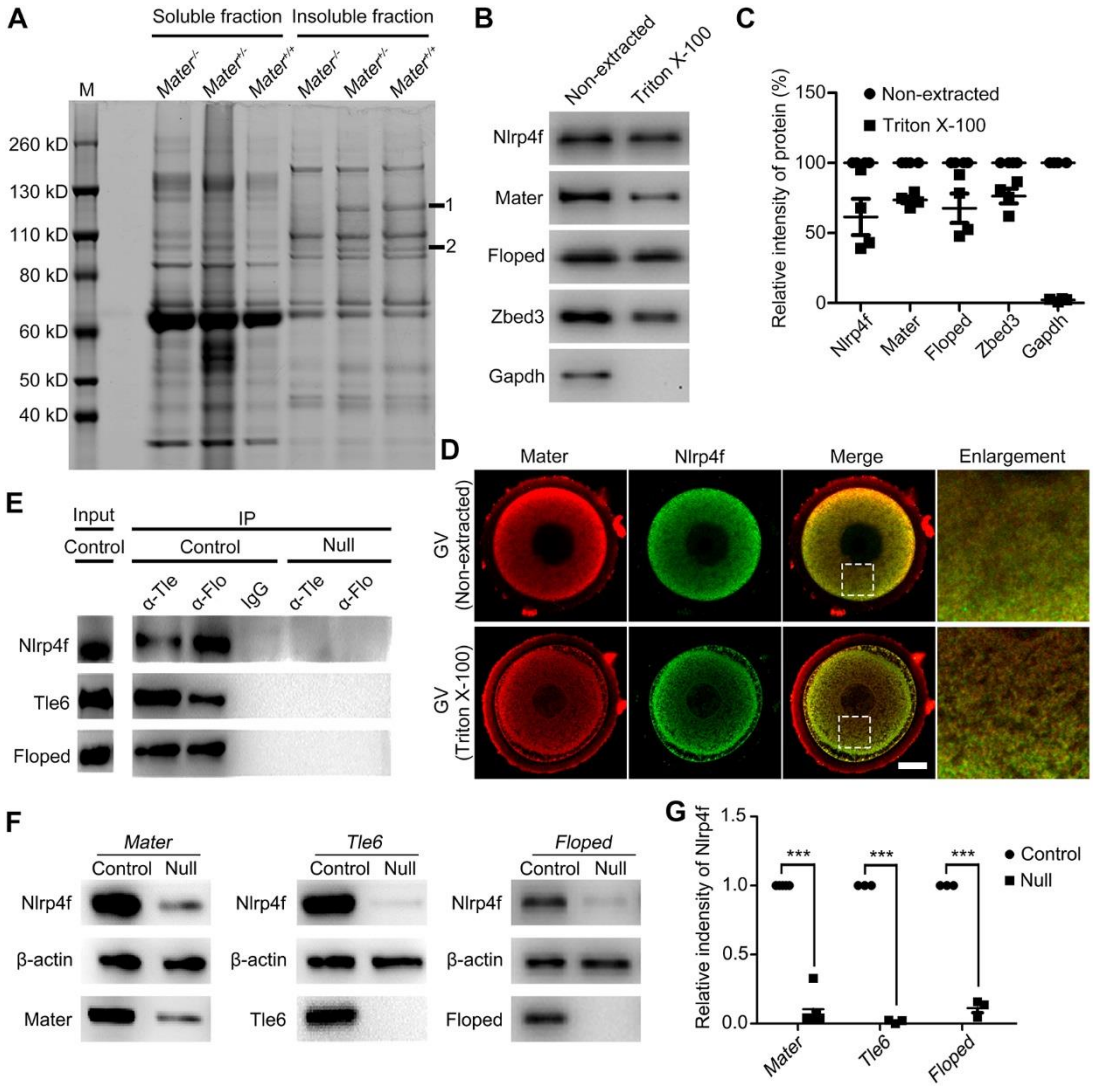

Figure 1. Identification of Nlrp4f as a novel component of the SCMC. (A) GV oocytes from *Mater*$^{+/+}$, *Mater*$^{+/-}$, *Mater*$^{-/-}$ were extracted with the buffer contained Triton X-100. The soluble and insoluble fractions were separated by SDS-PAGE and stained with Coomassie blue. Band 1 and 2 indicated the proteins in *Mater*$^{+/+}$ and *Mater*$^{+/-}$ oocytes but not in *Mater*$^{-/-}$ oocytes. (B) Normal mouse GV oocytes were treated with extraction buffer, followed by immunoblot with specific antibodies for the SCMC proteins. (C) Quantification of protein band intensities in B. Four independent experiments were performed. Error bars indicated SEM. (D) GV oocytes were isolated from normal females and treated with or without extraction buffer. These

oocytes were stained with anti-Mater (red) and anti-Nlrp4f antibodies (green). Scale bar, 20 μm. (E) Normal ovarian lysates were precipitated with anti-Tle6, anti-Floped antibodies, and IgG (negative control). The precipitated produces were examined by immunoblot with specific antibodies for Nlrp4f, Tle6 and Floped. Ovarian lysates from *Tle6* or *Floped* null mice were also used as negative controls. α-Tle, anti-Tle6 antibody. α-Flo, anti-Floped antibody. (F) GV oocytes were isolated from normal control, *Mater*$^{-/-}$, *Tle6*$^{-/-}$and *Floped*$^{-/-}$ females. The levels of SCMC proteins were examined by immunoblot with specific antibodies. β-actin was used as the loading control. (G) Quantification of Nlrp4f band intensity in *Mater*, *Tle6* and *Floped* null GV oocytes in F. Error bars, SEM, ***P < 0.001.

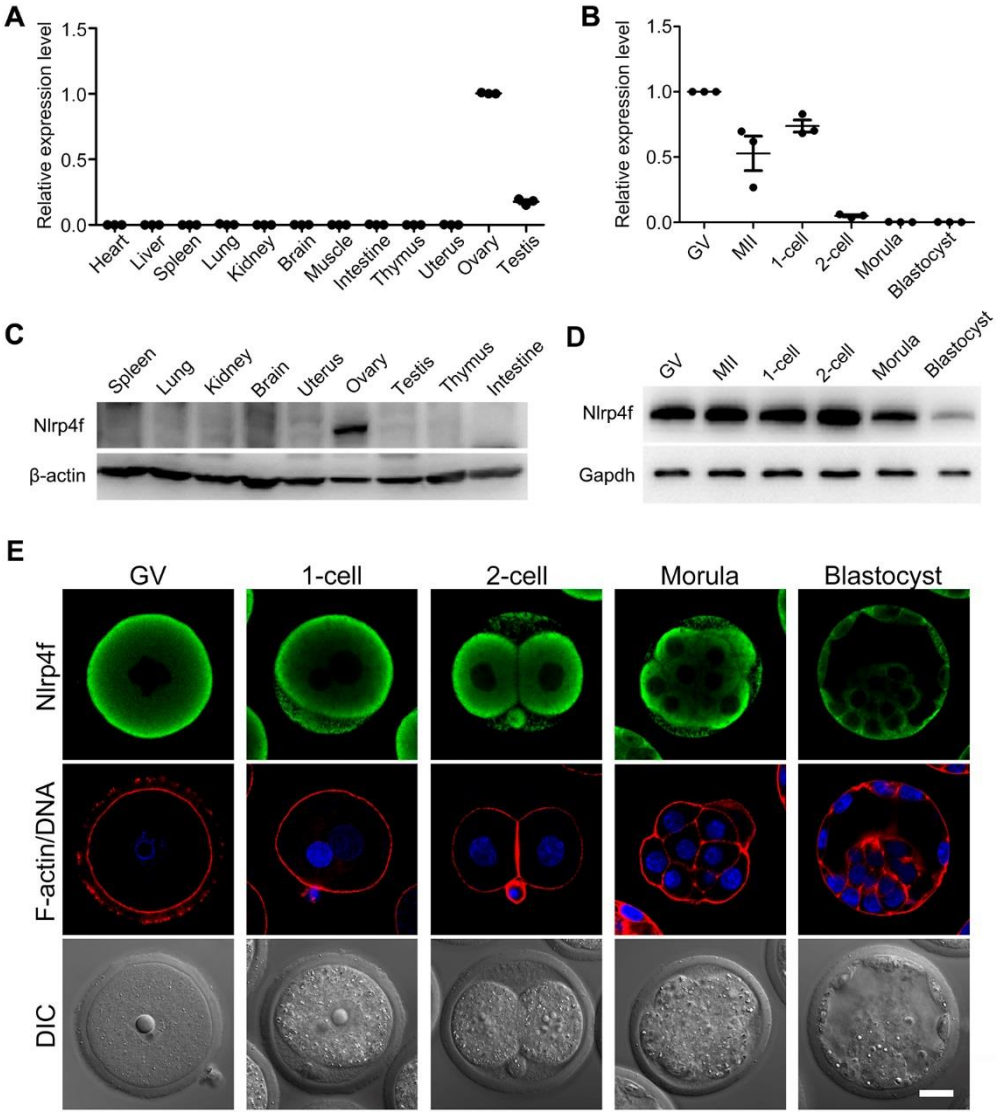

Figure 2. Expression patterns of *Nlrp4f* in the mouse. (A) *Nlrp4f* mRNA levels were determined by quantitative RT-PCR (qRT-PCR) in heart, liver, spleen, lung, kidney, brain, muscle, intestine, thymus, uterus, ovary, and testis from the adult mouse. The level of *Nlrp4f* mRNA expression in the ovary was set as 1. (B) qRT-PCR analysis of *Nlrp4f* mRNA expression in GV, MII oocytes, 1-cell, 2-cell, morula, and blastocyst embryos. The level of *Nlrp4f* mRNA expression in GV oocytes was set as 1. (C) Tissue lysates from mice at postnatal day 10 (PND 10) were examined by immunoblot with the specific antibodies for Nlrp4f and β-actin (loading control). (D)

Protiens were detected by immunoblot with the specific antibodies for Nlrp4f and Gapdh (loading control) in the oocytes and preimplantation embryos from normal females. (E) GV oocytes and preimplantation embryos were stained with anti-Nlrp4f antibody, Alexa Fluor™ 546 phalloidin (F-actin) and Hochest 33342 (DNA). Scale bar, 20 μm.

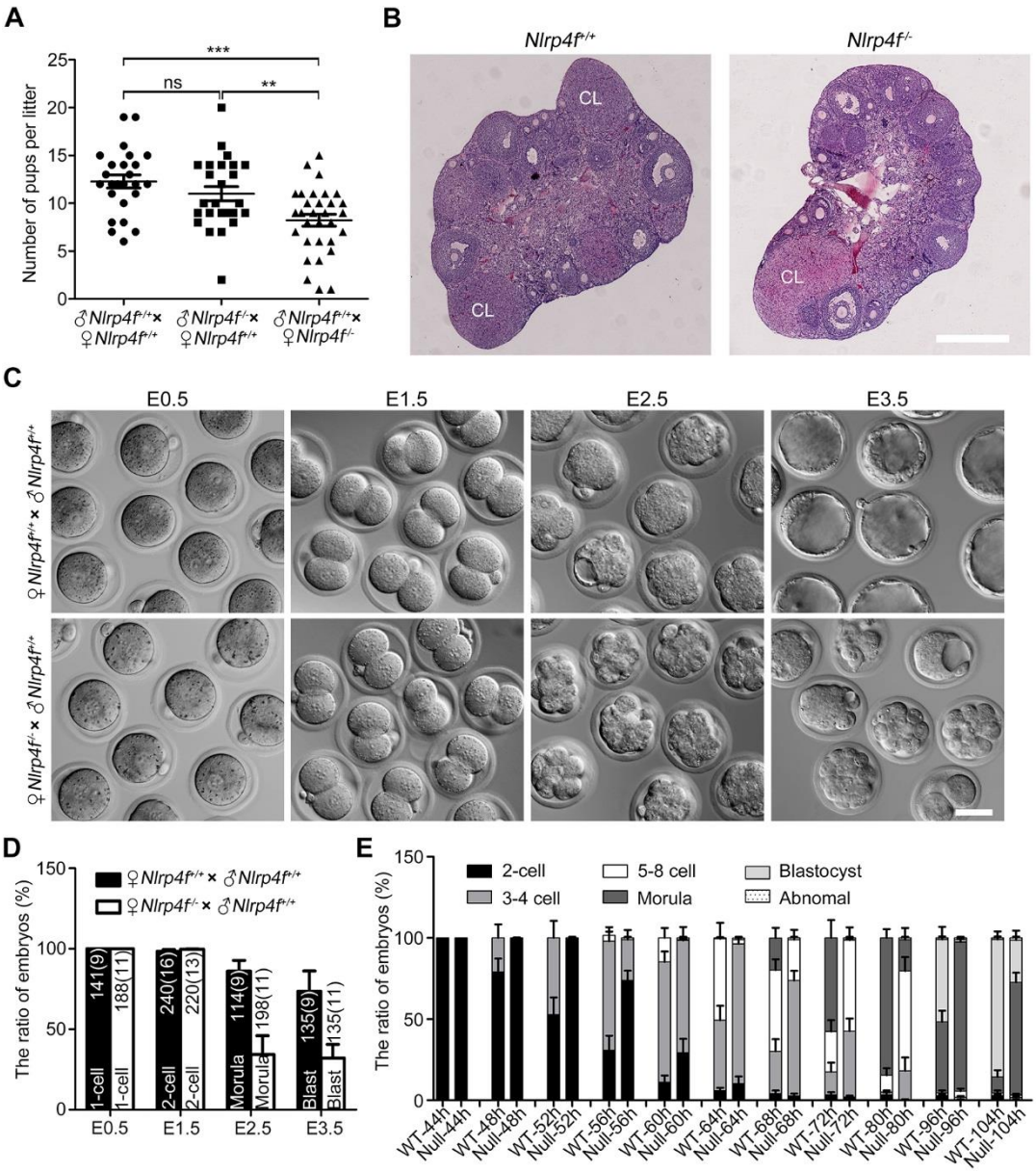

Figure 3. Depletion of Nlrp4f impairs female fertility and preimplantation development. (A) *Nlrp4f*$^{+/+}$ (WT), *Nlrp4f*$^{-/-}$ males mated with *Nlrp4f*$^{+/+}$ (WT) and *Nlrp4f*$^{-/-}$ females for three successive months. The litter size was recorded. Error bars, SEM. ns, no significant, **P < 0.01, ***P < 0.001. (B) Hematoxylin and eosin staining of ovarian sections from two-month-old *Nlrp4f*$^{+/+}$ and *Nlrp4f*$^{-/-}$ females. CL, corpus luteum. Scale bar, 500 μm. (C) Representative images of the bright field of embryos

flushed from control and *Nlrp4f*$^{-/-}$ females at E0.5, E1.5, E2.5, and E3.5, respectively. Scale bar, 50 μm. (D) The quantification of *in vivo* preimplantation embryos (1-cells, 2-cells, morulae, and blastocysts) after they were collected from *Nlrp4f*$^{+/+}$ and *Nlrp4f*$^{-/-}$ females at specific time points. The numbers in the graph reflected the number of analyzed embryos (number of females). Blast, blastocyst. (E) Two-cell embryos (234 from 16 *Nlrp4f*$^{+/+}$ females and 219 from 13 *Nlrp4f*$^{-/-}$ females in three independent experiments) were *in vitro* cultured for 60 hrs. Embryonic progression of different stages was morphologically assessed every four hours. The data represented the ratio of different stage embryos at 4-hour intervals.

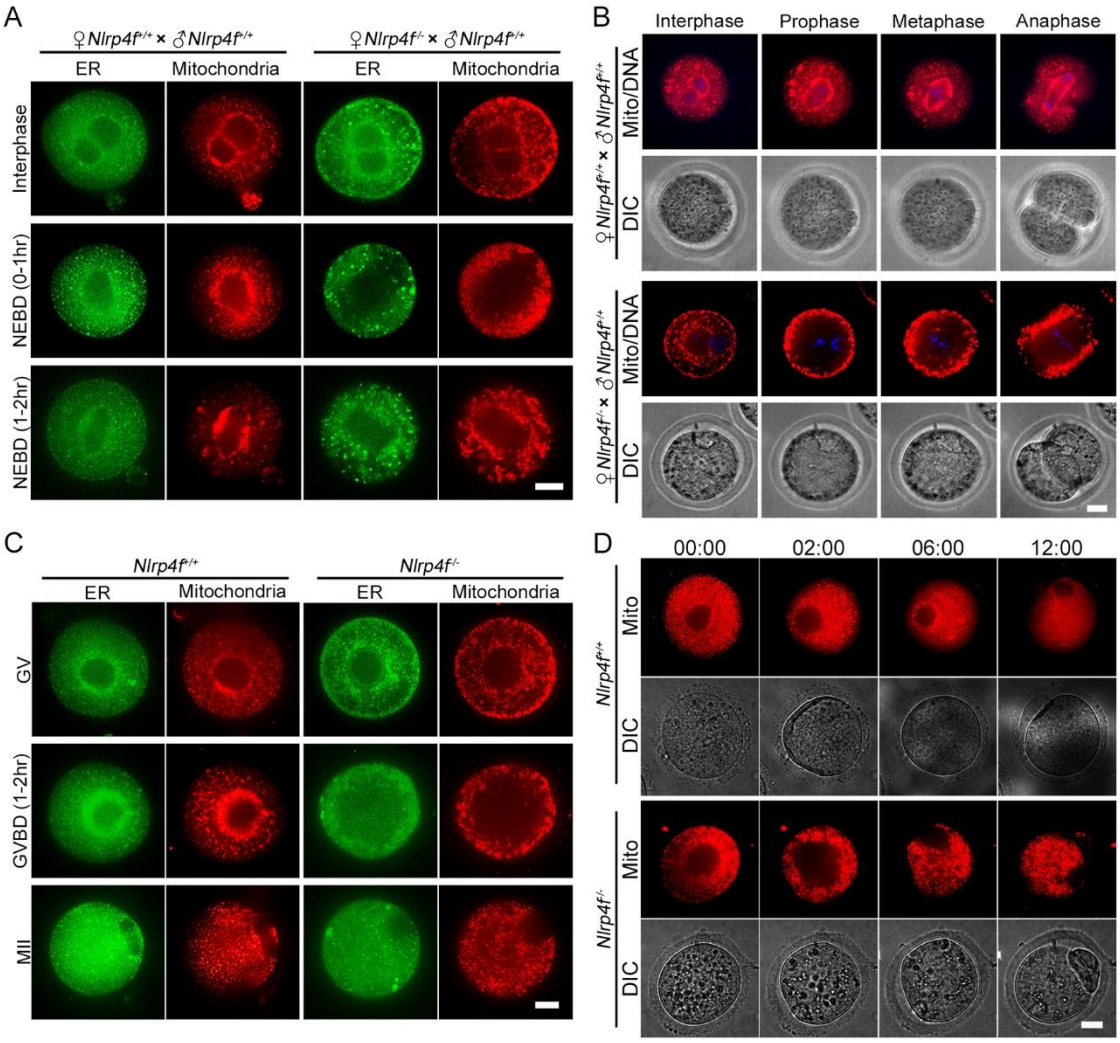

Figure 4. Disordered organelle distribution in the zygotes and oocytes with depletion of Nlrp4f. (A) The zygotes were isolated from *Nlrp4f*$^{+/+}$ (control) and *Nlrp4f*$^{-/-}$ (null) females after mating with normal fertile males. ERs and mitochondria were labeled with ER-Tracker (green) and MitoTracker (red) in the zygote from *Nlrp4f*$^{+/+}$ and *Nlrp4f*$^{-/-}$ females. Control (interphase, n = 29; NEBD 0-1 hr, n = 27; NEBD 1-2 hr, n = 15) and Nlrp4f null (interphase, n = 38; NEBD 0-1 hr, N = 22; NEBD 1-2 hr, n = 22) zygotes were examined in three independent experiments. Scale bar, 20 μm. (B) The zygotes from *Nlrp4f*$^{+/+}$ (control) and *Nlrp4f*$^{-/-}$ (Nlrp4f null) females were labeled with MitoTracker for mitochondria and Hochest 33342 for DNA.

These embryos were performed for live imaging with UltraVIEW-VoX. The stages of embryos were determined by DNA staining and morphology. Scale bar, 20 μm. (C) The oocytes were isolated from *Nlrp4f*$^{+/+}$ (control) and *Nlrp4f*$^{-/-}$ (null) females and were labeled with ER-Tracker (green) and MitoTracker (red) for ERs and mitochondria. Control (GV, n = 14; GVBD 1-2 hrs, n = 40; MII, n = 68) and null (GV, n = 33; GVBD 1-2 hrs, n = 77; MII, n = 74) oocytes were investigated in four independent experiments. Scale bar, 20 μm. (D) Live imaging of the maturation of oocytes after they were labeled with MitoTracker for mitochondria. Scale bar, 20 μm.

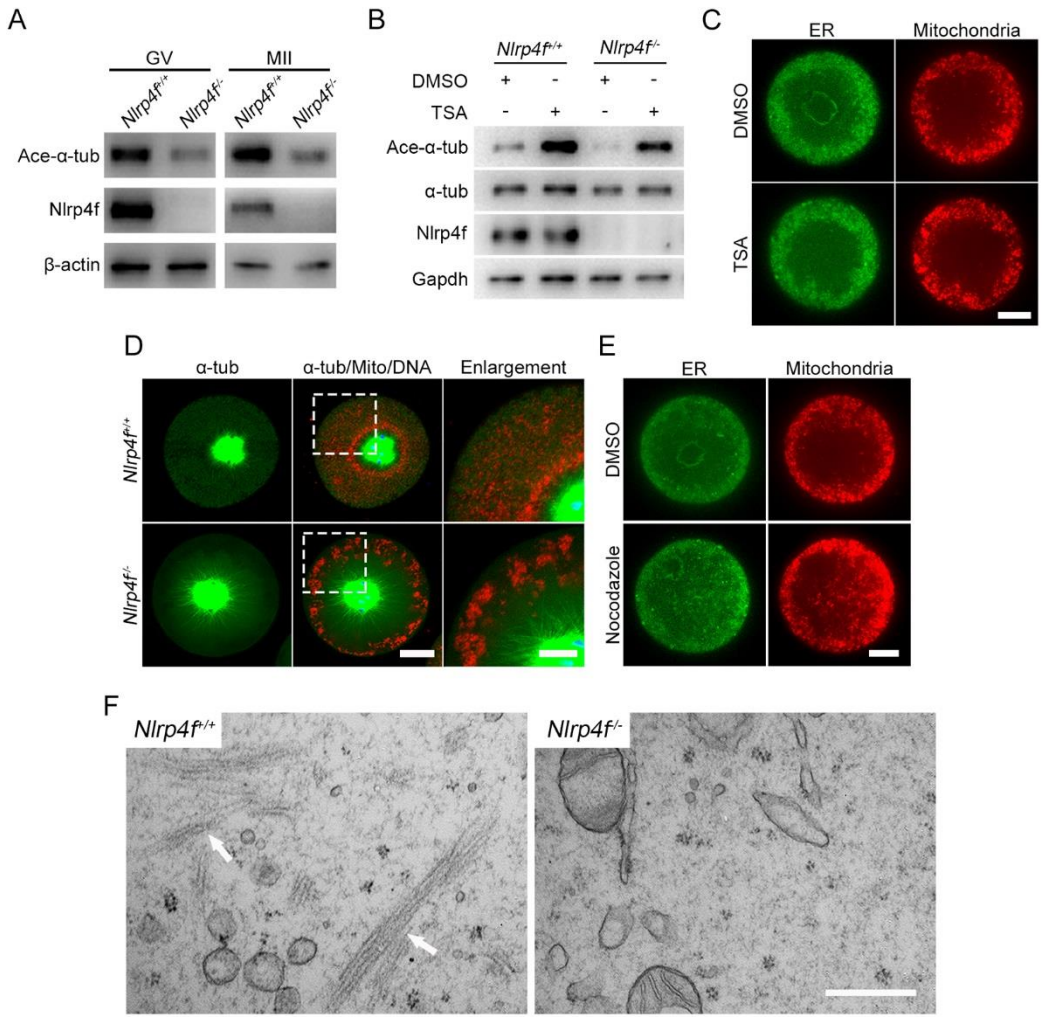

Figure 5. Abnormal formation of microtubules and CPLs in *Nlrp4f*$^{-/-}$ oocytes. (A) Immunoblot of acetylated α-tubulin, Nlrp4f and β-actin in GV and MII oocytes from *Nlrp4*$^{+/+}$ and *Nlrp4f*$^{-/-}$ females. Ace-α-tub, Acetylated α-tubulin antibody. (B) GV oocytes were isolated from *Nlrp4*$^{+/+}$ and *Nlrp4f*$^{-/-}$ females and were treated with DMSO and TSA. Immunoblot was performed for these oocytes at GVBD 1-2 hrs with the antibodies for acetylated α-tubulin, α-tubulin, Nlrp4f, and Gapdh. Ace-α-tub, Acetylated α-tubulin antibody, α-tub, α-tubulin antibody. (C) ERs and mitochondria were labeled with ER-Tracker (green) and MitoTracker (red) in *Nlrp4*$^{+/+}$ and *Nlrp4f*$^{-/-}$ oocytes treating with DMSO and TSA after GVBD (1-2 hrs). Scale bar, 20 μm. (D)

Nlrp4f$^{+/+}$ and *Nlrp4f*$^{-/-}$ oocytes were labeled with MitoTracker (red) at GVBD 1-2 hours, then fixed and stained with α-tubulin-FITC (green). Scale bar, 20 μm. The astral-like microtubules from spindles were enlarged and showed on the right. Scale bar, 10 μm. α-tub, α-tubulin antibody. Mito, mitochondria. (E) ERs and mitochondria were labeled with ER-Tracker (green) and MitoTracker (red) in *Nlrp4*$^{+/+}$ and *Nlrp4f*$^{-/-}$ oocytes treating with DMSO and Nocodazole after GVBD (1-2 hrs). Scale bar, 20 μm. (F) The ovaries of *Nlrp4f*$^{+/+}$ and *Nlrp4f*$^{-/-}$ females were fixed and sectioned for transmission electron microscopy (TEM). Representative images of the oocytes from these ovaries were obtained by JEM-1230. White arrows indicate the cytoplasmic lattices (CPLs). Scale bar, 500 nm.

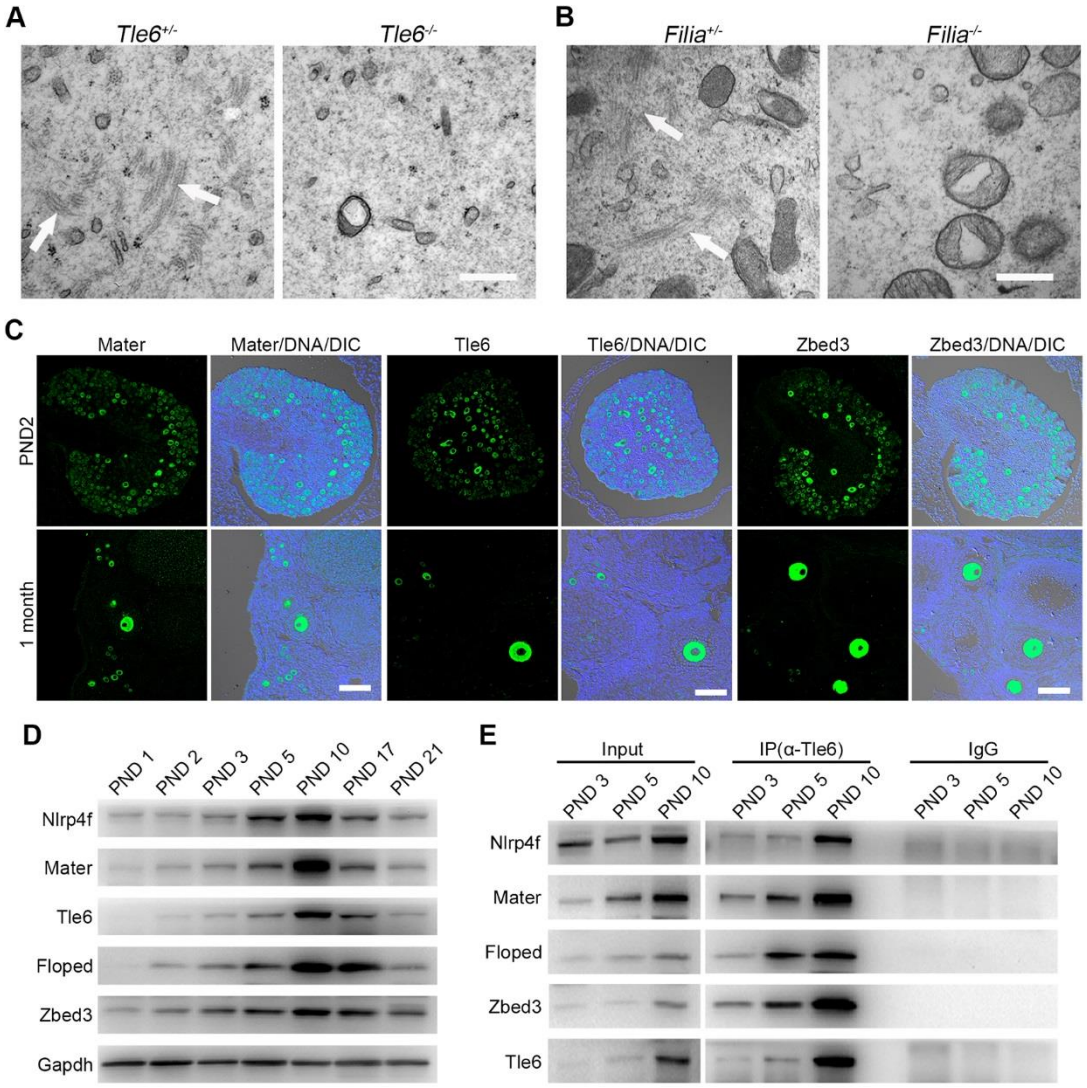

Figure 6. The formation of CPLs and SCMC in mouse oocytes. (A) TEM results of GV oocytes from *Tle6*$^{+/-}$ and *Tle6*$^{-/-}$ ovaries. White arrows indicate CPLs. Scale bar, 500 nm. (B) TEM results of GV oocytes from *Filia*$^{+/-}$ and *Filia*$^{-/-}$ ovaries. White arrows indicate CPLs. Scale bar, 500 nm. (C) Paraffin sections of ovaries from postnatal day (PND) 2 and one-month-old normal mice were stained with anti-Mater, -Tle6, -Zbed3 antibodies and Hochest 33342 (DNA). Scale bar, 100 μm. (D) Ovarian lysates were extracted from normal females of different ages (PND 1, PND 2, PND 3, PND 5, PND 10, PND 17 and PND 21) and examined by immunoblot with anti-Nlrp4f, -Mater, -Tle6,

-Floped and -Zbed3 antibodies, respectively. (E) Normal ovarian lysates of different ages (PND 3, PND 5, and PND 10) were immunoprecipitated with anti-Tle6 antibodies or normal IgG (mouse), followed by immunoblot with specific antibodies.

Figure S1

A

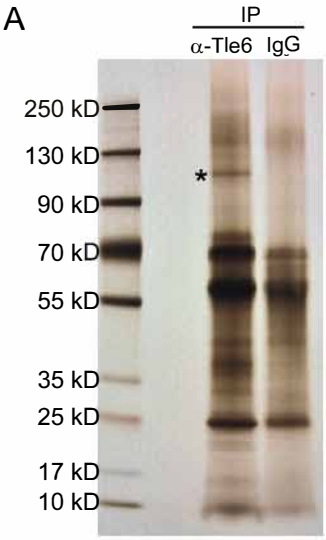

B

Proteins	Score	Coverage	Peptides	MV(kDa)
MATER	80.69	39.06	36	125.4
TLE6	51.80	44.92	20	65.0
FLOPED	5.44	25.00	4	18.4
FILIA	22.77	42.49	12	37.9
ZBED3	11.76	34.21	9	25.6
NLRP4F	22.54	18.89	14	107.8

Figure S1. Identification of Nlrp4f as a potential component of the SCMC by mass spectrometry (Modified from our previous report (Gao et al., 2018)). (A) Normal GV oocytes were precipitated with anti-Tle6 antibody, and IgG (negative control). The precipitated produces were separated by SDS-PAGE, examined by silver staining and analyzed by mass spectrometry. The asterisk indicated the possible band of Nlrp4f estimated by its molecular weight. (B) The information of mass spectrometry was shown for the known SCMC components and Nlrp4f.

Figure S2

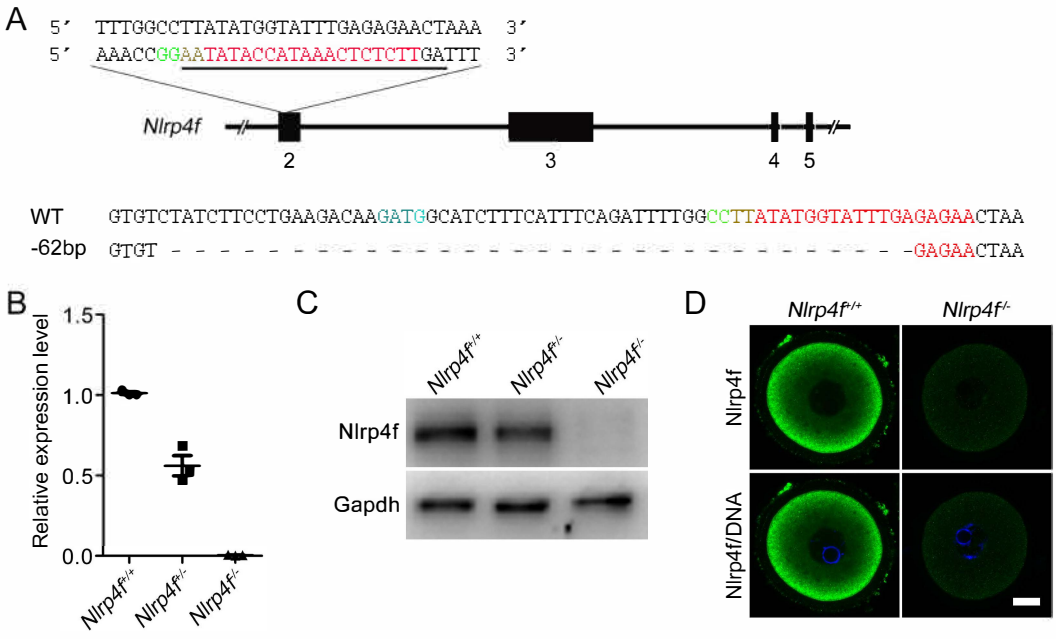

Figure S2. Generation of *Nlrp4f* knockout mice. (A) A schematic of the generation of *Nlrp4f* knockout mice using CRISPR/Cas9. The black rectangles are exons. The sgRNA-targeting sequence is underlined and shown in red, and the protospacer-adjacent motif (PAM) sequence is in green. The initiation codon ATG was labeled in blue. The sequences of normal (WT) and mutant alleles of the founder mice were also shown. (B) qRT-PCR analysis of *Nlrp4f* mRNA expression in *Nlrp4f*$^{+/+}$, *Nlrp4f*$^{+/-}$ and *Nlrp4f*$^{-/-}$ oocytes. The data was normalized to the abundance of *Gapdh* mRNA. The results were from three independent experiments. (C) Immunoblot analysis of Nlrp4f expression in *Nlrp4f*$^{+/+}$, *Nlrp4f*$^{+/-}$ and *Nlrp4f*$^{-/-}$ MII oocytes. Gapdh was used as an internal reference. (D) Immunofluorescent staining of GV oocytes from *Nlrp4f*$^{+/+}$ and *Nlrp4f*$^{-/-}$ mice with Nlrp4f antibody and Hochest 33342 (DNA). Scale bar, 20 μm.

Figure S3

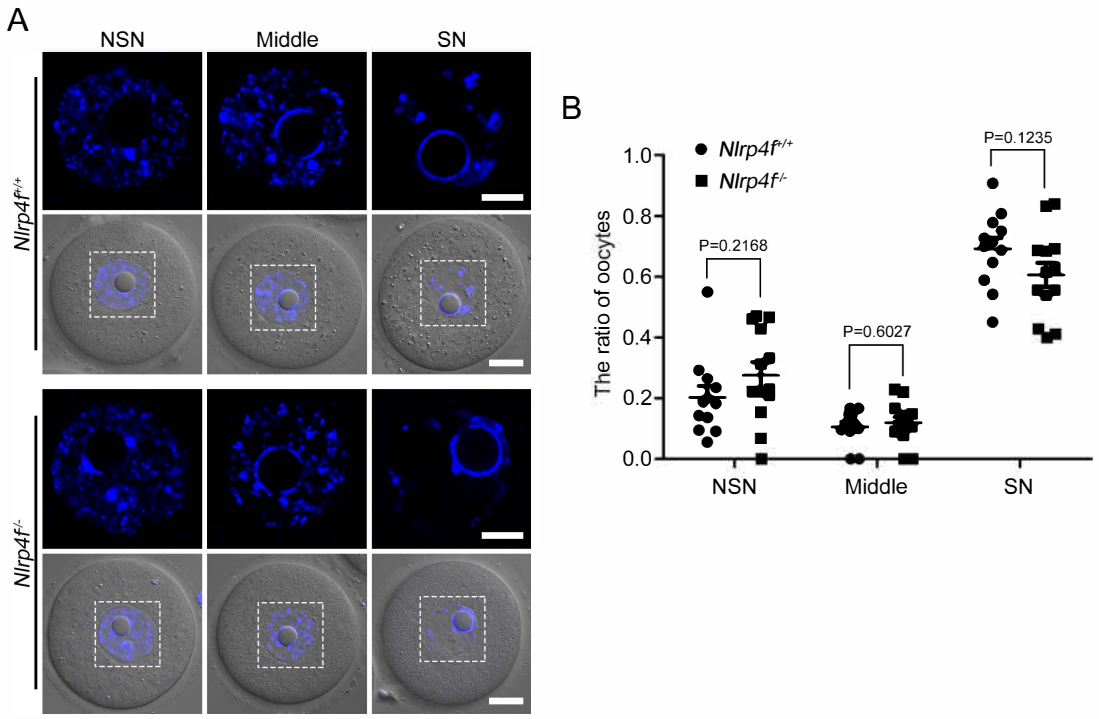

Figure S3. Chromatin configurations in fully grown oocytes. (A) Fully grown oocytes from *Nlrp4f*$^{+/+}$ and *Nlrp4f*$^{+/-}$ females were stained with Hochest 33342 for DNA. According to their chromatin configuration of DNA, the oocytes were classified into three types, NSN, Middle and SN type. The nucleus was dotted with white color and magnified. Scale bar in the upper panel, 10 μm. Scale bar in the down panel, 20 μm. (B) GV oocytes from *Nlrp4f*$^{+/+}$ (n = 12) and *Nlrp4f*$^{-/-}$ (n = 13) female mice were classified into three groups, and the ratio was calculated by the number of NSN, Middle and SN dividing the number of total oocytes. Error bars, SEM.

Figure S4

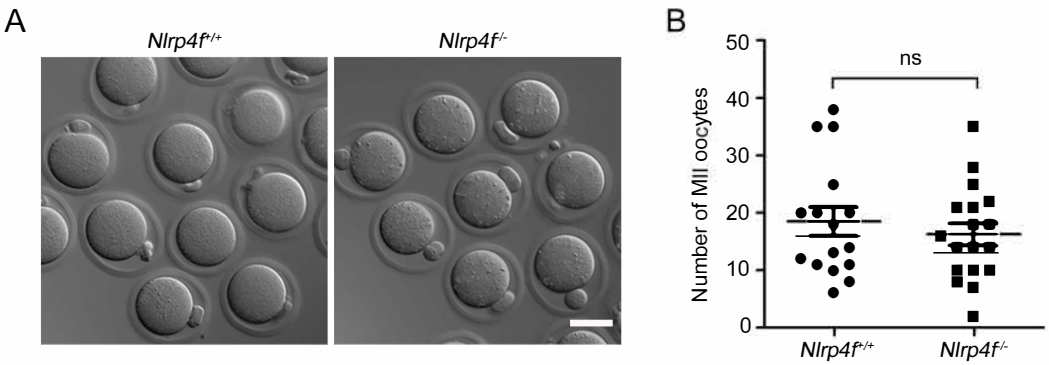

Figure S4. Ovulation in *Nlrp4f* null mice. (A) Representative images of bright field of *Nlrp4f*$^{+/+}$ and *Nlrp4f*$^{-/-}$ MII oocytes after superovulation. Scale bar, 50 μm. (B) The number of MII oocytes from *Nlrp4f*$^{+/+}$ and *Nlrp4f*$^{-/-}$ mice after superovulation. ns, no significant.

Figure S5

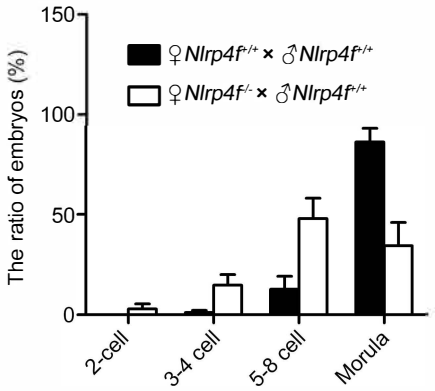

Figure S5. Abnormal development in embryos with depletion of maternal Nlrp4f. The ratio of embryos at different development stages from control and *Nlrp4f*$^{-/-}$ females at E2.5.

Figure S6

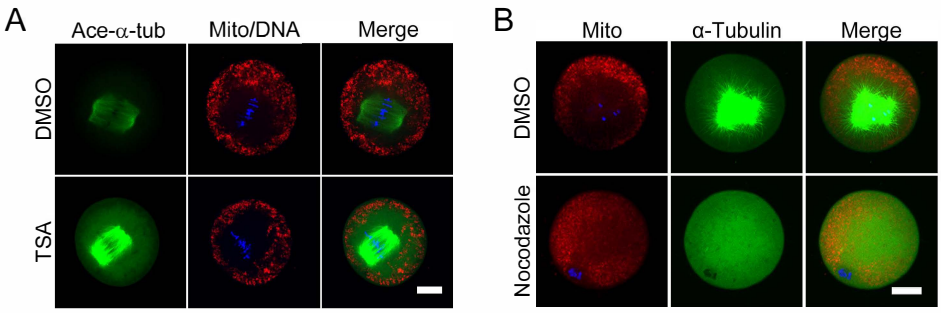

Figure S6. Drug treatment of *Nlrp4f*$^{-/-}$ oocytes. (A) *Nlrp4f*$^{-/-}$ oocytes were labeled with MitoTracker (red) after the treatment with DMSO or TSA at GVBD 1-2 hrs, then fixed and stained with anti-acetylated-α-tubulin antibody (Ace-α-tubulin, green) and Hochest 33342 (DNA, blue). Scale bar, 20 μm. (B) *Nlrp4f*$^{-/-}$ oocytes were labeled with MitoTracker (red) the treatment with DMSO or Nocodazole at GVBD 1-2 hrs, then fixed and stained with anti-α-tubulin antibody (green) and Hochest33342 (DNA, blue). Scale bar, 20 μm.

Figure S7

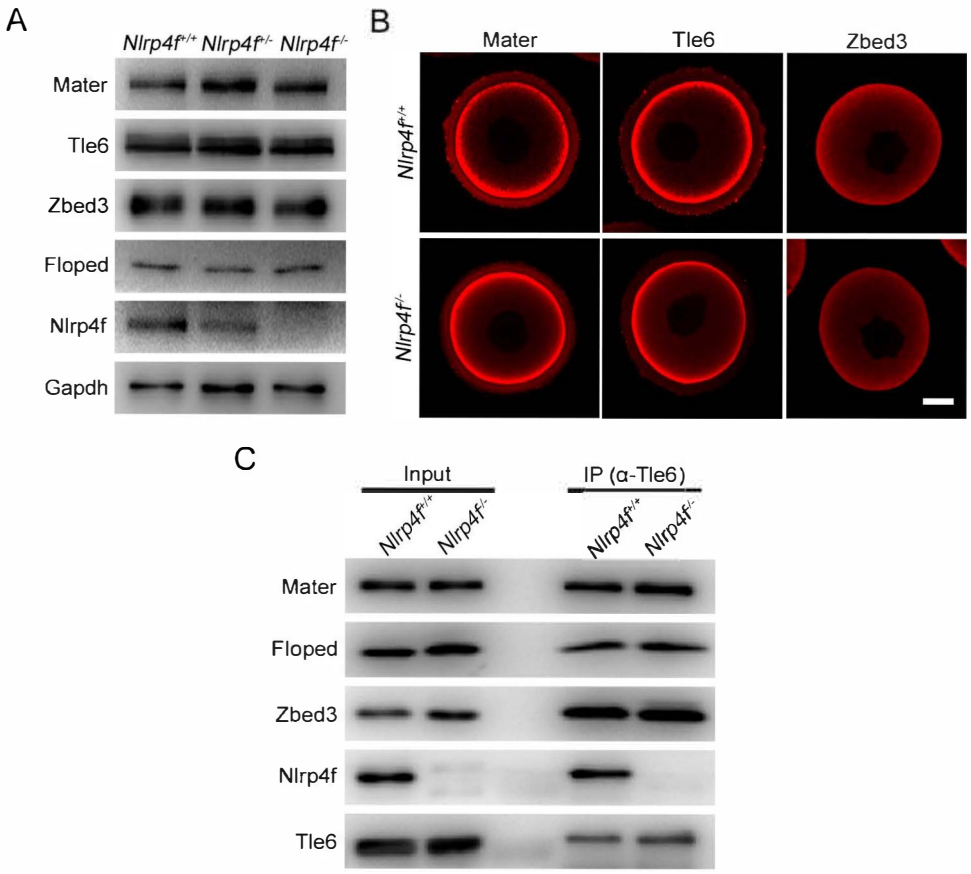

Figure S7. The expression patterns of the known SCMC components in *Nlrp4f*$^{-/-}$ oocytes. (A) Immunoblot of *Nlrp4f*$^{+/+}$, *Nlrp4f*$^{+/-}$ and *Nlrp4f*$^{-/-}$ GV oocytes with anti-Mater, -Tle6, -Zbed3, -Floped and -Nlrp4f antibodies. Gapdh was used as a loading control. (B) Immunofluorescent staining of GV oocytes from *Nlrp4f*$^{+/+}$ and *Nlrp4f*$^{-/-}$ females with anti-Mater, -Tle6 and -Zbed3 antibodies. Scale bar, 20 μm. (C) Co-immunoprecipitation of GV oocytes (200) from *Nlrp4f*$^{+/+}$ and *Nlrp4f*$^{-/-}$ females with anti-Tle6 antibody, followed by immunoblot with specific antibodies for the SCMC proteins.

Figure S8

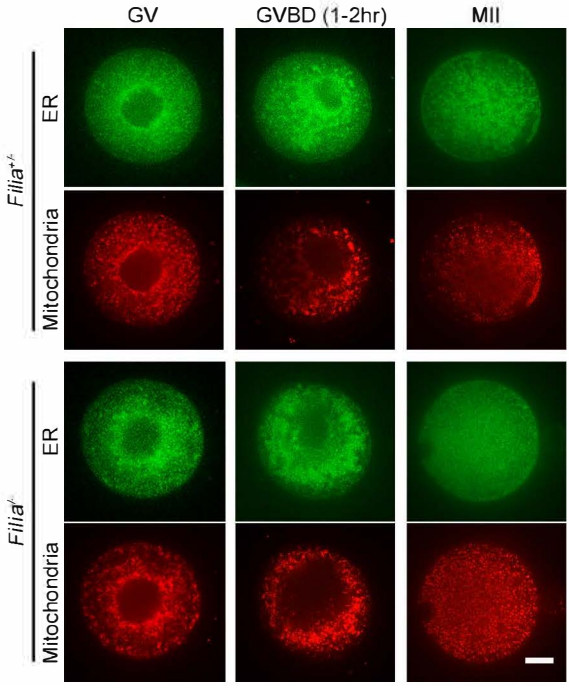

Figure S8. Disordered organelle distribution in *Filia*$^{-/-}$ oocytes. The oocytes were isolated from *Filia*$^{+/-}$ (control) and *Filia*$^{-/-}$ (null) females and were labeled with ER-Tracker (green) and MitoTracker (red) for ERs and mitochondria. Control (GV, n = 18; GVBD 1-2 hrs, n = 19; MII, n = 22) and null (GV, n = 24; GVBD 1-2 hrs, n = 31; MII, n = 34) oocytes were investigated in three independent experiments. Scale bar, 20 μm.

Table S1 The list of antibodies

Primary antibodies			
Antibody	For immunoblot	For immunofluorescence	Source
Mouse anti-MATER	1:1000	1:200	
Mouse anti-TLE6	1:1000	1:200	
Rabbit anti-FLOPED	1:2000	-	
Rabbit anti-ZBED3	1:2000	1:200	
Sheep anti-Filia	1:500	-	
Rabbit anti-NLRP4F	1:2000	1:200	Produced by Abmart
Mouse anti-GAPDH	1:5000	-	Sungene biotech, KM9002T
Mouse anti-β-actin	1:5000	-	Sungene biotech, KM9001T
Mouse anti-Acetylated-α-tubulin	1:1000	-	Abcam, ab24610
Rabbit anti-α-tubulin	1:1000	-	Cell signaling, 2144
Mouse anti-α-Tubulin-FITC	-	1:200	Sigma, F2168

Secondary antibodies			
Antibody	For immunoblot	For immunofluorescence	Source
Alexa Fluor® 488 AffiniPure Donkey Anti-Rabbit IgG	-	1:500	Jackson Immuno Research, 711-545-152
Alexa Fluor® 594 AffiniPure Donkey Anti-Mouse IgG	-	1:500	Jackson Immuno Research, 715-585-150
Peroxidase AffiniPure Goat Anti-Rabbit IgG	1:5000	-	Jackson Immuno Research, 111-035-003
Peroxidase AffiniPure Goat Anti-Mouse IgG	1:5000	-	Jackson Immuno Research, 115-035-003
Peroxidase AffiniPure Donkey Anti-Sheep IgG	1:2000	-	Jackson Immuno Research, 713-035-003

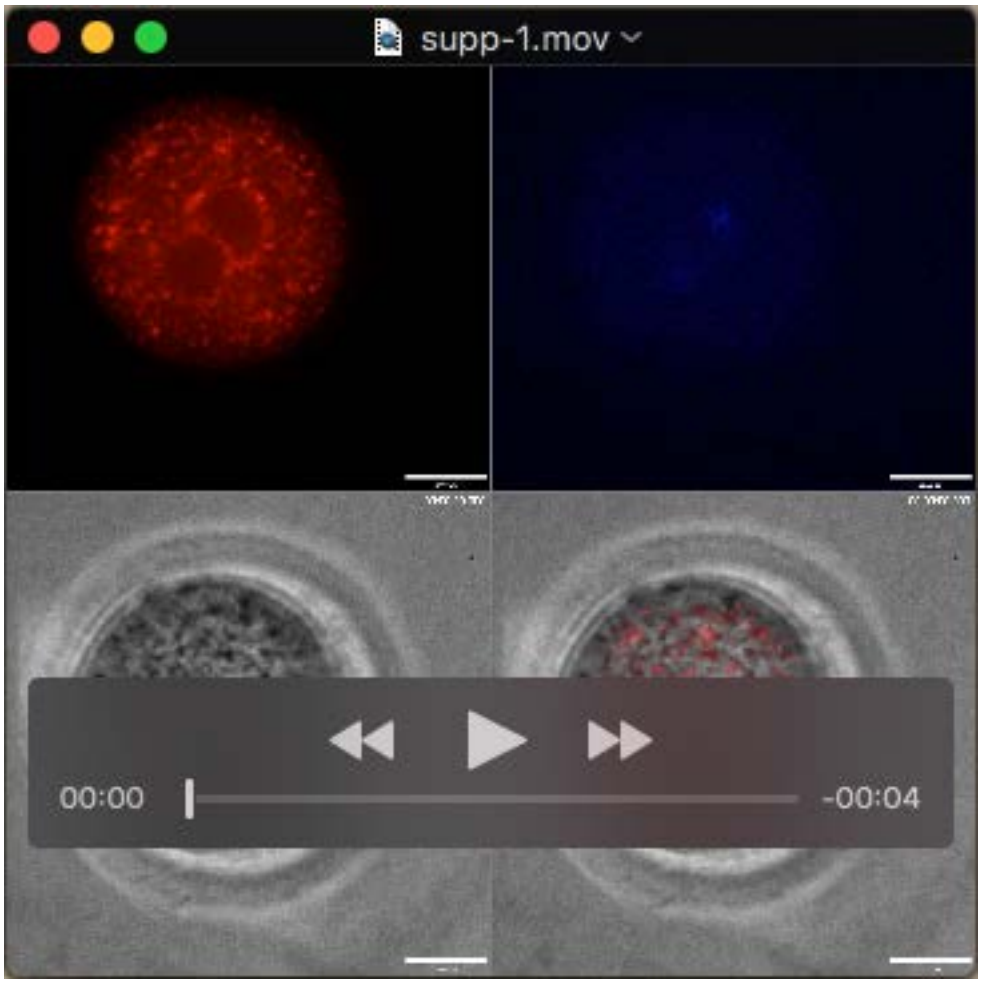

Movie 1. Mitochondria dynamics in the embryos from *Nlrp4f*$^{+/+}$ females during 1-cell to 2-cell development. Zygotes were isolated from *Nlrp4f*$^{+/+}$ females at 24 hrs after hCG stimulation, labeled with MitoTracker for mitochondria and Hochest 33342 for DNA and cultured to 2-cell stage. Time-lapse images were captured every 30 mins with UltraVIEW-VoX. Related to Fig. 4B.

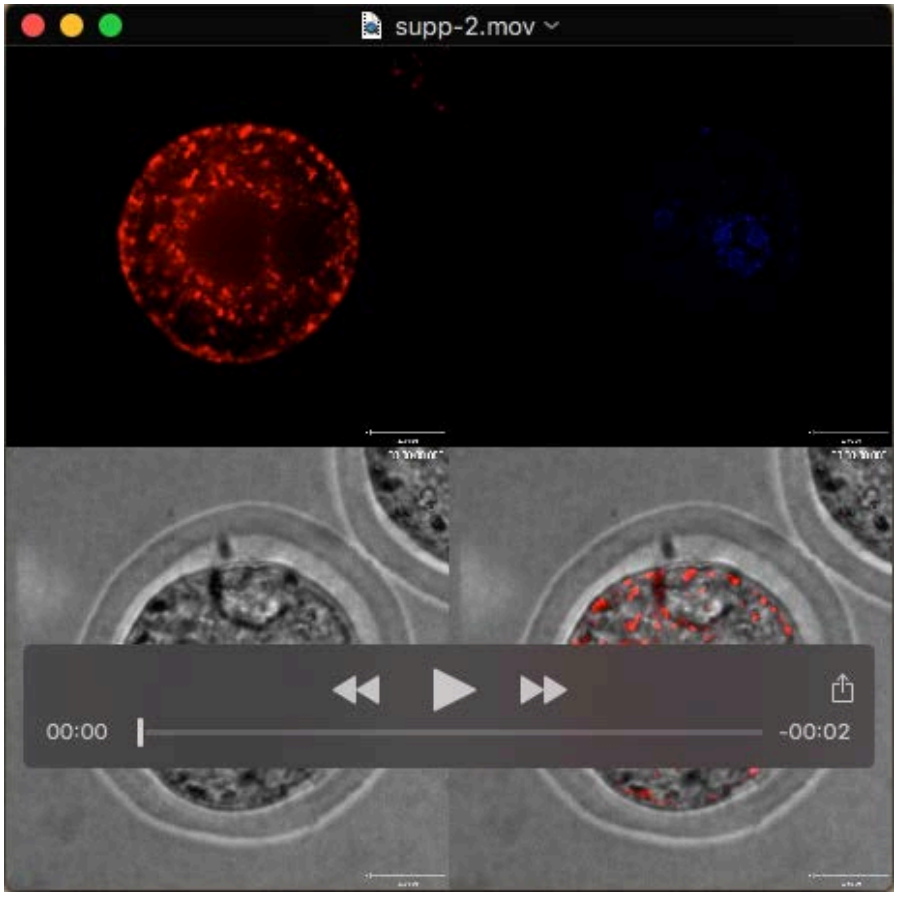

Movie 2. Mitochondria dynamics in the embryos from *Nlrp4f*$^{-/-}$ females during 1-cell to 2-cell development. Zygotes were isolated from *Nlrp4f*$^{-/-}$ females at 26 hrs after hCG stimulation, labeled with MitoTracker for mitochondria and Hochest 33342 for DNA and cultured to 2-cell stage. Time-lapse images were captured every 30 mins with UltraVIEW-VoX. Related to Fig. 4B.

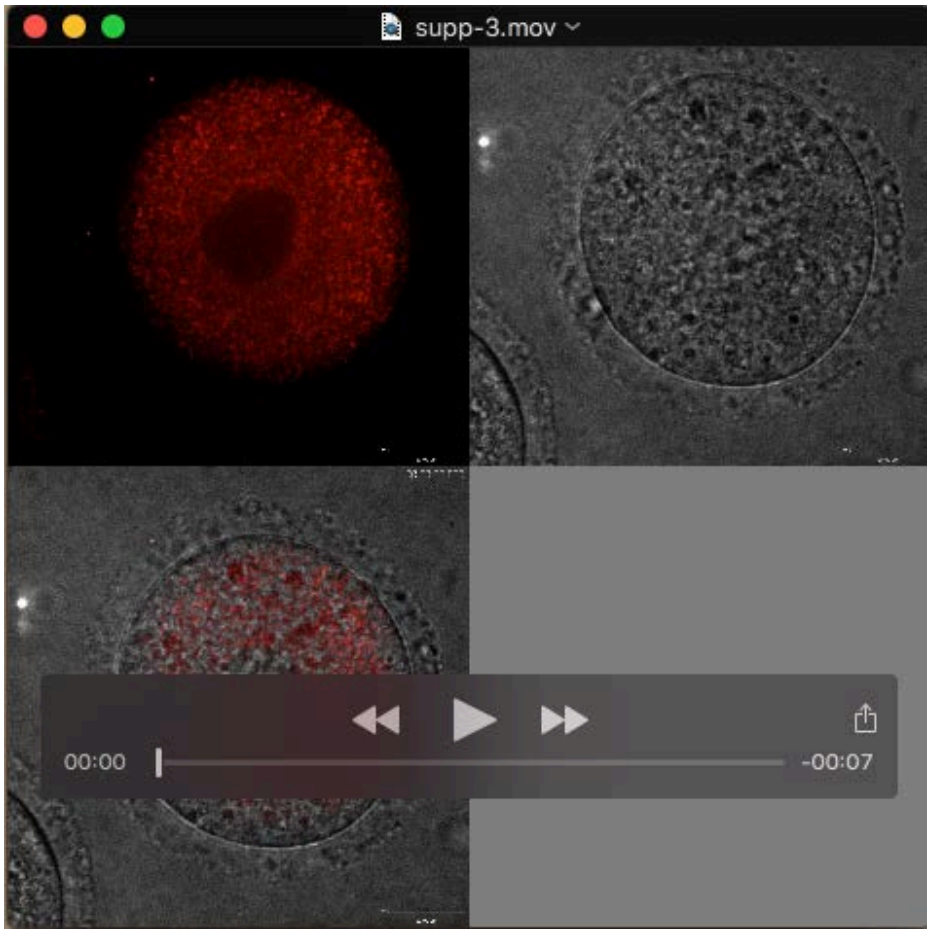

Movie 3. Mitochondria dynamics in the oocytes from *Nlrp4f*$^{+/+}$ females during GV to MII maturation. GV *Nlrp4f*$^{+/+}$ oocytes were labeled with MitoTracker for mitochondria and cultured to MII stage. Time-lapse images were captured every 30 mins with UltraVIEW-VoX. Related to Fig. 4D.

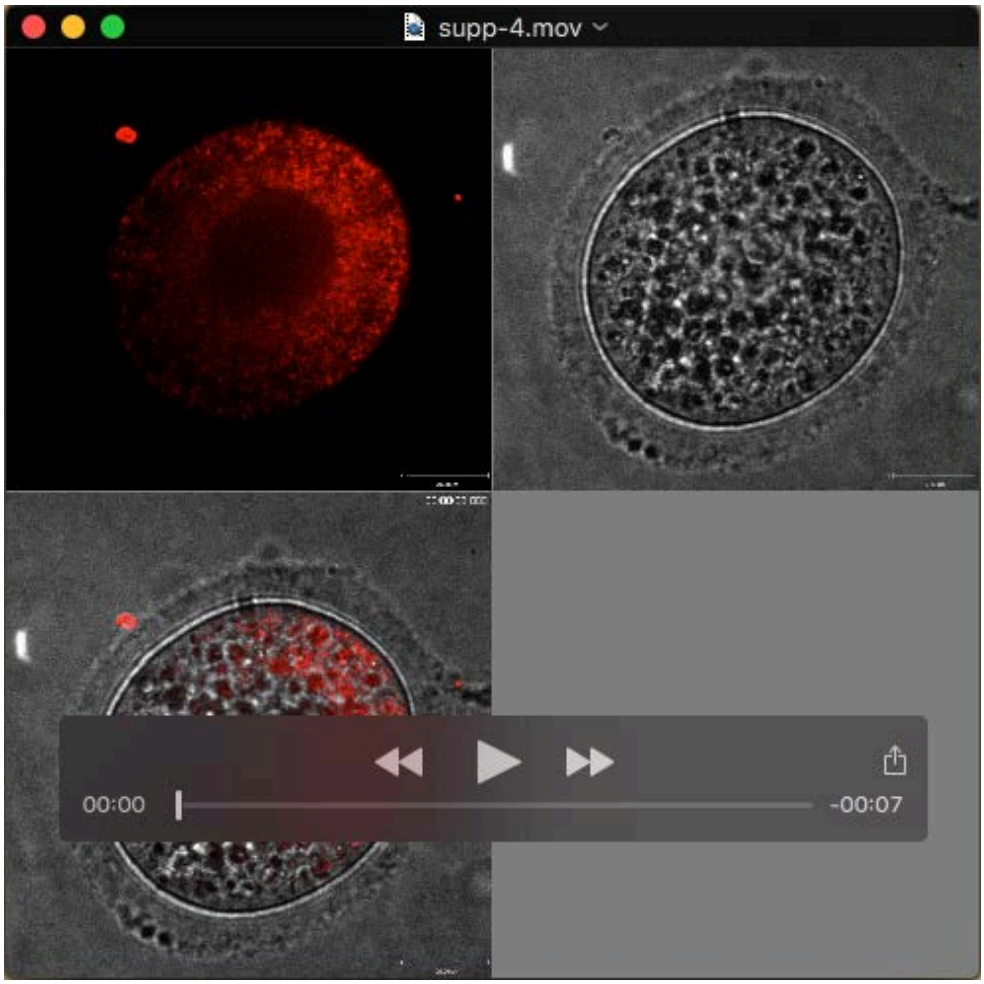

Movie 4. Mitochondria dynamics in the oocytes from *Nlrp4f*$^{-/-}$ females during GV to MII maturation. *Nlrp4f*$^{-/-}$ GV oocytes were labeled with MitoTracker for mitochondria and cultured to MII stage. Time-lapse images were captured every 30 mins with UltraVIEW-VoX. Related to Fig. 4D.

Figure S1

A

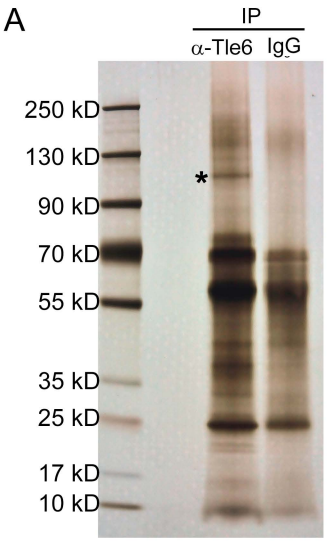

B

Proteins	Score	Coverage	Peptides	MV(kDa)
Nlrp5	80.69	39.06	36	125.4
Tle6	51.80	44.92	20	65.0
Ooep	5.44	25.00	4	18.4
Khdc3	22.77	42.49	12	37.9
Zbed3	11.76	34.21	9	25.6
Nlrp4f	22.54	18.89	14	107.8

Figure S1. Identification of Nlrp4f as a potential component of the SCMC by mass spectrometry (Modified from our previous report (Gao et al., 2018)). (A) Normal GV oocytes were precipitated with anti-Tle6 antibody, and IgG (negative control). The precipitated produces were separated by SDS-PAGE, examined by silver staining and analyzed by mass spectrometry. The asterisk indicated the possible band of Nlrp4f estimated by its molecular weight. (B) The information of mass spectrometry was shown for the known SCMC components and Nlrp4f.

Figure S2

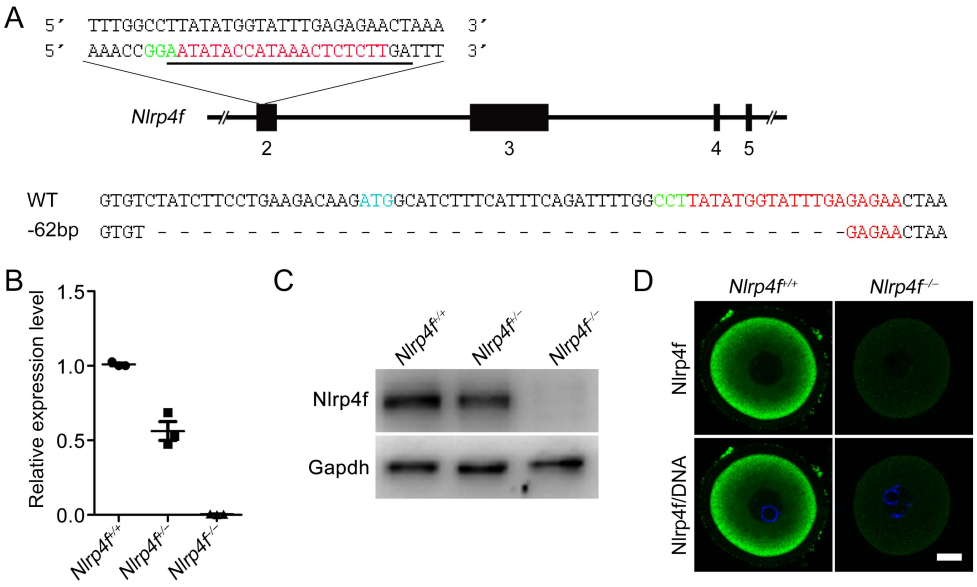

Figure S2. Generation of *Nlrp4f* knockout mice. (A) A schematic of the generation of *Nlrp4f* knockout mice using CRISPR/Cas9. The black rectangles are exons. The sgRNA-targeting sequence is underlined and shown in red, and the protospacer-adjacent motif (PAM) sequence is in green. The initiation codon ATG was labeled in blue. The sequences of normal (WT) and mutant alleles of the founder mice were also shown. (B) qRT-PCR analysis of *Nlrp4f* mRNA expression in *Nlrp4f*$^{+/+}$, *Nlrp4f*$^{-/+}$ and *Nlrp4f*$^{-/-}$ oocytes. The data was normalized to the abundance of *Gapdh* mRNA. The results were from three independent experiments. (C) Immunoblot analysis of Nlrp4f expression in *Nlrp4f*$^{+/+}$, *Nlrp4f*$^{-/+}$ and *Nlrp4f*$^{-/-}$ MII oocytes. Gapdh was used as an internal reference. (D) Immunofluorescent staining of GV oocytes from *Nlrp4f*$^{+/+}$ and *Nlrp4f*$^{-/-}$ mice with Nlrp4f antibody and Hochest 33342 (DNA). Scale bar: 20 μm.

Figure S3

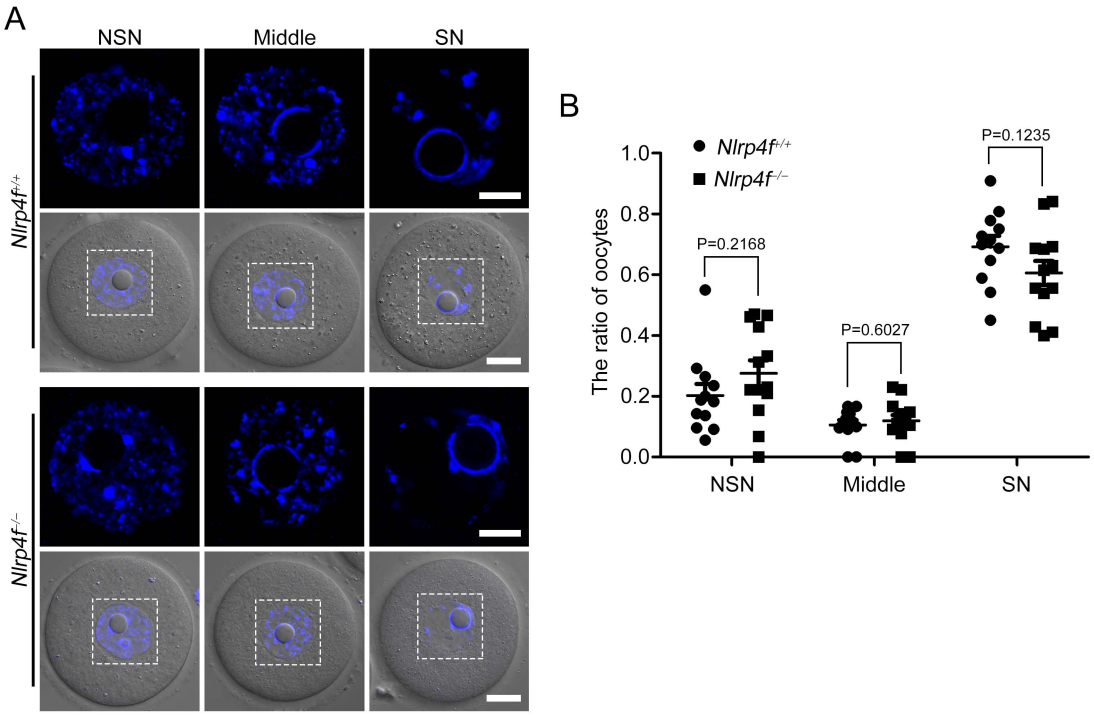

Figure S3. Chromatin configurations in fully grown oocytes. (A) Fully grown oocytes from *Nlrp4f*$^{+/+}$ and *Nlrp4f*$^{-/-}$ females were stained with Hochest 33342 for DNA. According to their chromatin configuration of DNA, the oocytes were classified into three types, NSN, Middle and SN type. The nucleus was dotted with white color and magnified. Scale bar in the upper panel: 10 μm. Scale bar in the down panel: 20 μm. (B) GV oocytes from *Nlrp4f*$^{+/+}$ (n = 12) and *Nlrp4f*$^{-/-}$ (n = 13) female mice were classified into three groups, and the ratio was calculated by the number of NSN, Middle and SN dividing the number of total oocytes. Error bars, s.e.m.

Figure S4

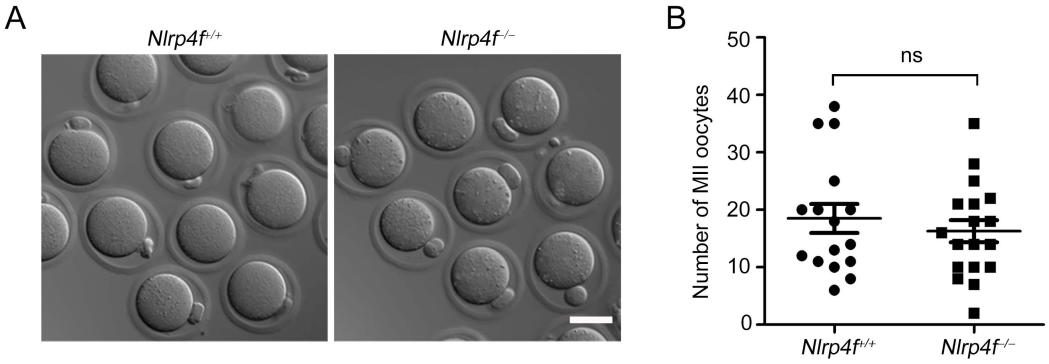

Figure S4. Ovulation in *Nlrp4f* null mice. (A) Representative images of bright field of *Nlrp4f*$^{+/+}$ and *Nlrp4f*$^{-/-}$ MII oocytes after superovulation. Scale bar: 50 μm. (B) The number of MII oocytes from *Nlrp4f*$^{+/+}$ and *Nlrp4f*$^{-/-}$ mice after superovulation. Error bars, s.e.m. ns, no significant.

Figure S5

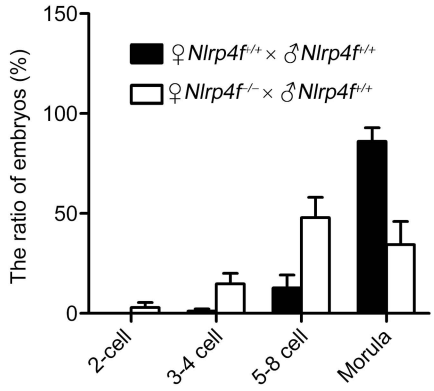

Figure S5. Abnormal development in embryos with depletion of maternal Nlrp4f. The ratio of embryos at different development stages from *Nlrp4f*$^{+/+}$ and *Nlrp4f*$^{-/-}$ females at E2.5.

Figure S6

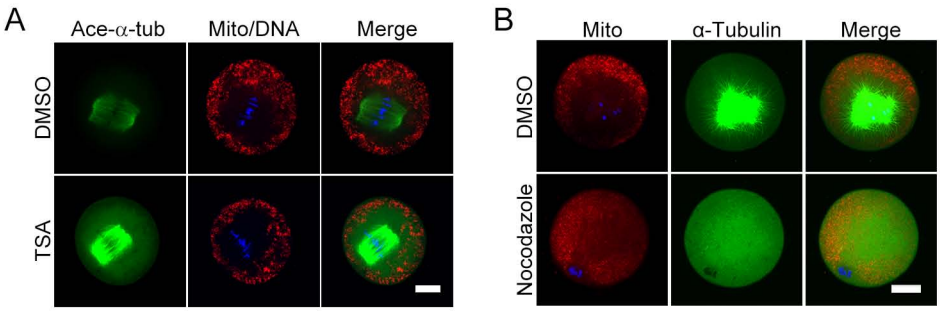

Figure S6. Drug treatment of *Nlrp4f*$^{-/-}$ oocytes. (A) *Nlrp4f*$^{-/-}$ oocytes were labeled with MitoTracker (red) after the treatment with DMSO or TSA at GVBD 1-2 h, then fixed and stained with anti-acetylated-α-tubulin antibody (Ace-α-tubulin, green) and Hochest 33342 (DNA, blue). Scale bar: 20 μm. (B) *Nlrp4f*$^{-/-}$ oocytes were labeled with MitoTracker (red) the treatment with DMSO or Nocodazole at GVBD 1-2 h, then fixed and stained with anti-α-tubulin antibody (green) and Hochest33342 (DNA, blue). Scale bar: 20 μm.

Figure S7

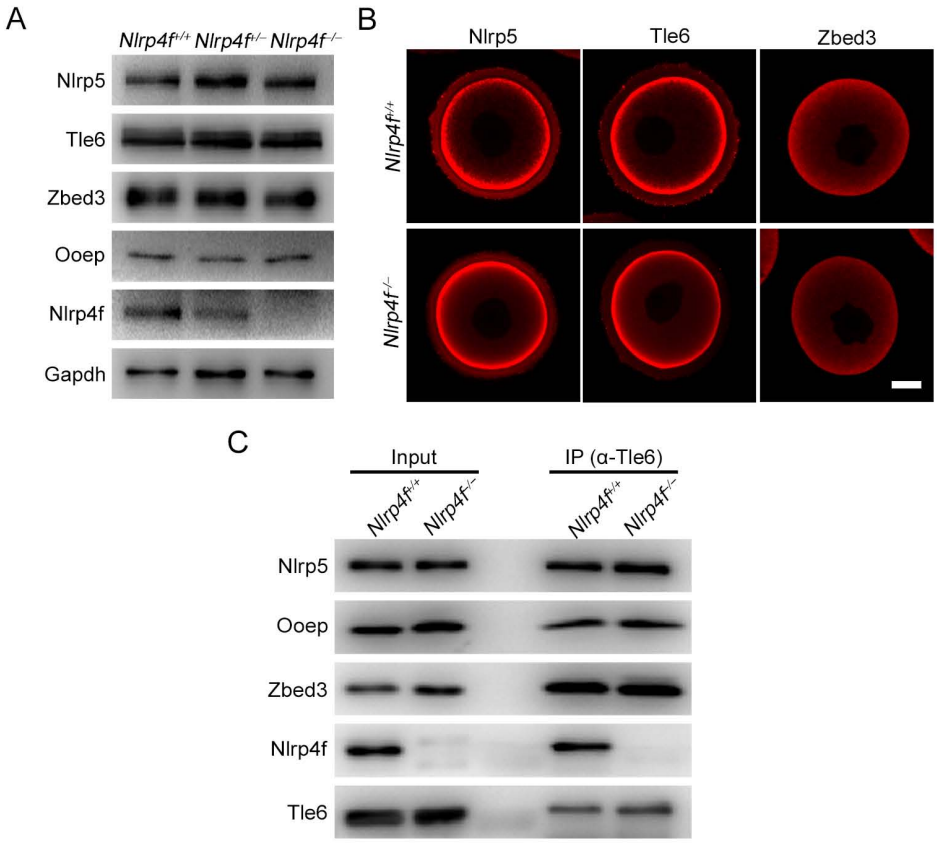

Figure S7. The expression patterns of the known SCMC components in *Nlrp4f*$^{-/-}$ oocytes. (A) Immunoblot of *Nlrp4f*$^{+/+}$, *Nlrp4f*$^{-/+}$ and *Nlrp4f*$^{-/-}$ GV oocytes with anti-Nlrp5, -Tle6, -Zbed3, -Ooep and -Nlrp4f antibodies. Gapdh was used as a loading control. (B) Immunofluorescent staining of GV oocytes from *Nlrp4f*$^{+/+}$ and *Nlrp4f*$^{-/-}$ females with anti-Nlrp5, -Tle6 and -Zbed3 antibodies. Scale bar: 20 μm. (C) Co-immunoprecipitation of GV oocytes (200) from *Nlrp4f*$^{+/+}$ and *Nlrp4f*$^{-/-}$ females with anti-Tle6 antibody, followed by immunoblot with specific antibodies for the SCMC proteins.

Figure S8

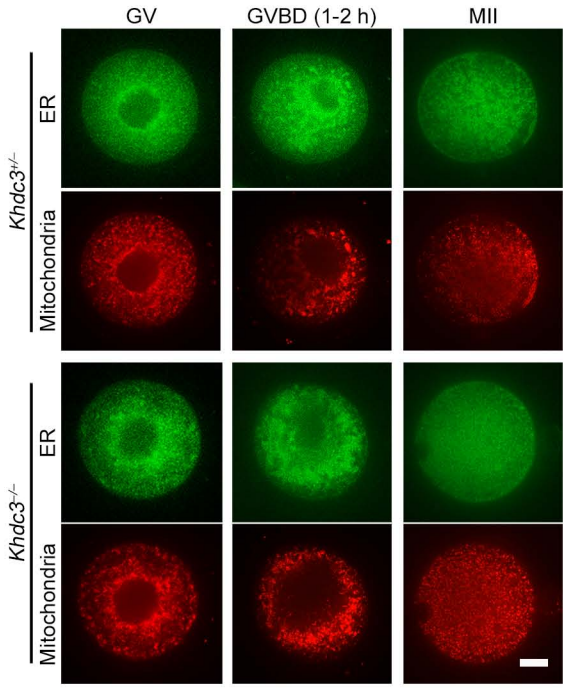

Figure S8. Disordered organelle distribution in *Khdc3*$^{-/-}$ oocytes. The oocytes were isolated from *Khdc3*$^{+/-}$ and *Khdc3*$^{-/-}$ females and were labeled with ER-Tracker (green) and MitoTracker (red) for ERs and mitochondria. *Khdc3*$^{-/+}$ (GV, n = 18; GVBD 1-2 h, n = 19; MII, n = 22) and *Khdc3*$^{-/-}$ (GV, n = 24; GVBD 1-2 h, n = 31; MII, n = 34) oocytes were investigated in three independent experiments. Scale bar: 20 μm.

Table 1 The list of antibodies

Primary antibodies			
Antibody	For immunoblot	For immunofluorescence	Source
Mouse anti-Nlrp5	1:1000	1:200	
Mouse anti-Tle6	1:1000	1:200	
Rabbit anti-Ooep	1:2000	-	
Rabbit anti-Zbed3	1:2000	1:200	
Sheep anti-Khdc3	1:500	-	
Rabbit anti-Nlrp4f	1:2000	1:200	Produced by Abmart
Mouse anti-Gapdh	1:5000	-	Sungene biotech, KM9002T
Mouse anti-β-actin	1:5000	-	Sungene biotech, KM9001T
Mouse anti-Acetylated-α-tubulin	1:1000	-	Abcam, ab24610
Rabbit anti-α-tubulin	1:1000	-	Cell signaling, 2144
Mouse anti-α-tubulin-FITC	-	1:200	Sigma, F2168

Secondary antibodies			
Antibody	For immunoblot	For immunofluorescence	Source
Alexa Fluor® 488 AffiniPure Donkey Anti-Rabbit IgG	-	1:500	Jackson Immuno Research, 711-545-152
Alexa Fluor® 594 AffiniPure Donkey Anti-Mouse IgG	-	1:500	Jackson Immuno Research, 715-585-150
Peroxidase AffiniPure Goat Anti-Rabbit IgG	1:5000	-	Jackson Immuno Research, 111-035-003
Peroxidase AffiniPure Goat Anti-Mouse IgG	1:5000	-	Jackson Immuno Research, 115-035-003
Peroxidase AffiniPure Donkey Anti-Sheep IgG	1:2000	-	Jackson Immuno Research, 713-035-003

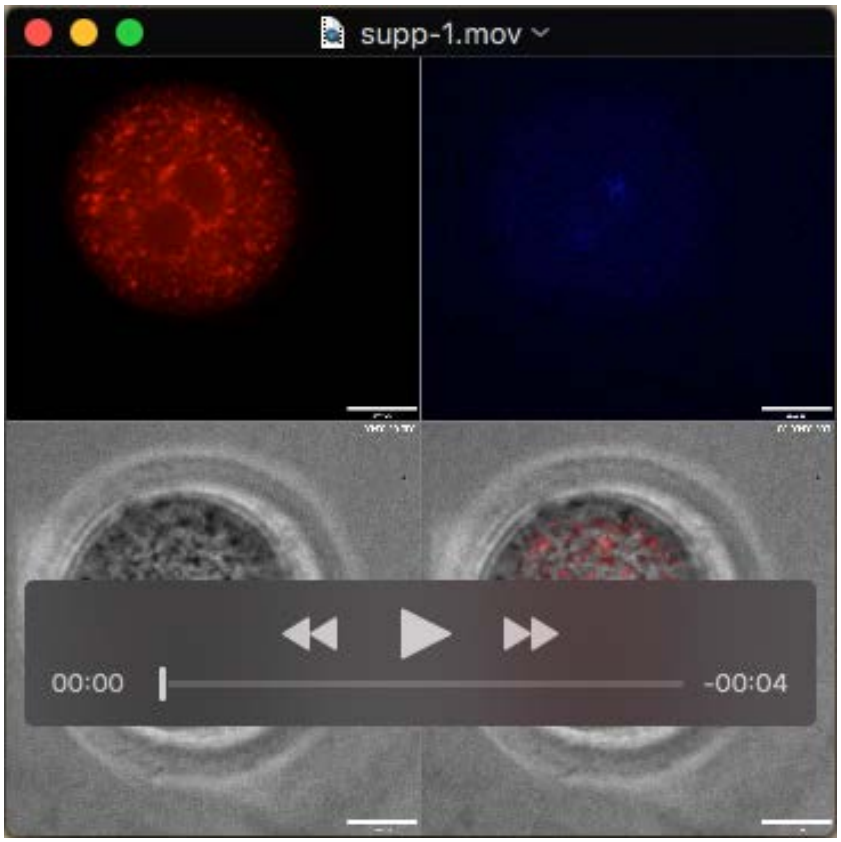

Movie 1. Mitochondria dynamics in the embryos from *Nlrp4f*$^{+/+}$ females during 1-cell to 2-cell development. Zygotes were isolated from *Nlrp4f*$^{+/+}$ females at 24 h after hCG stimulation, labeled with MitoTracker for mitochondria and Hochest 33342 for DNA and cultured to 2-cell stage. Time-lapse images were captured every 30 mins with UltraVIEW-VoX. Related to Fig. 4B.

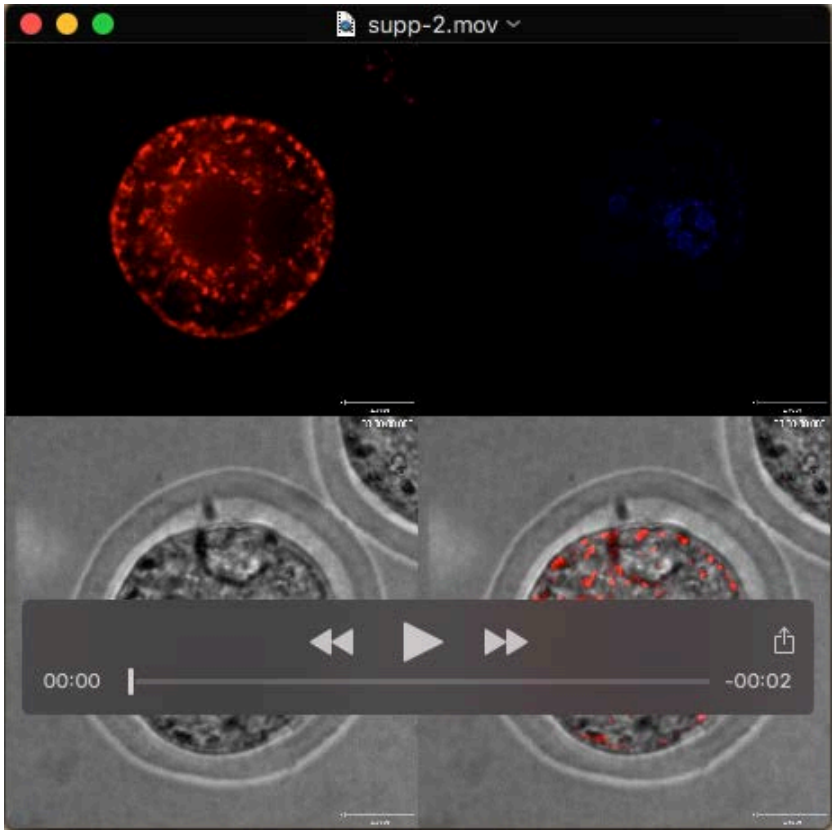

Movie 2. Mitochondria dynamics in the embryos from *Nlrp4f*$^{-/-}$ females during 1-cell to 2-cell development. Zygotes were isolated from *Nlrp4f*$^{-/-}$ females at 26 hrs after hCG stimulation, labeled with MitoTracker for mitochondria and Hochest 33342 for DNA and cultured to 2-cell stage. Time-lapse images were captured every 30 mins with UltraVIEW-VoX. Related to Fig. 4B.

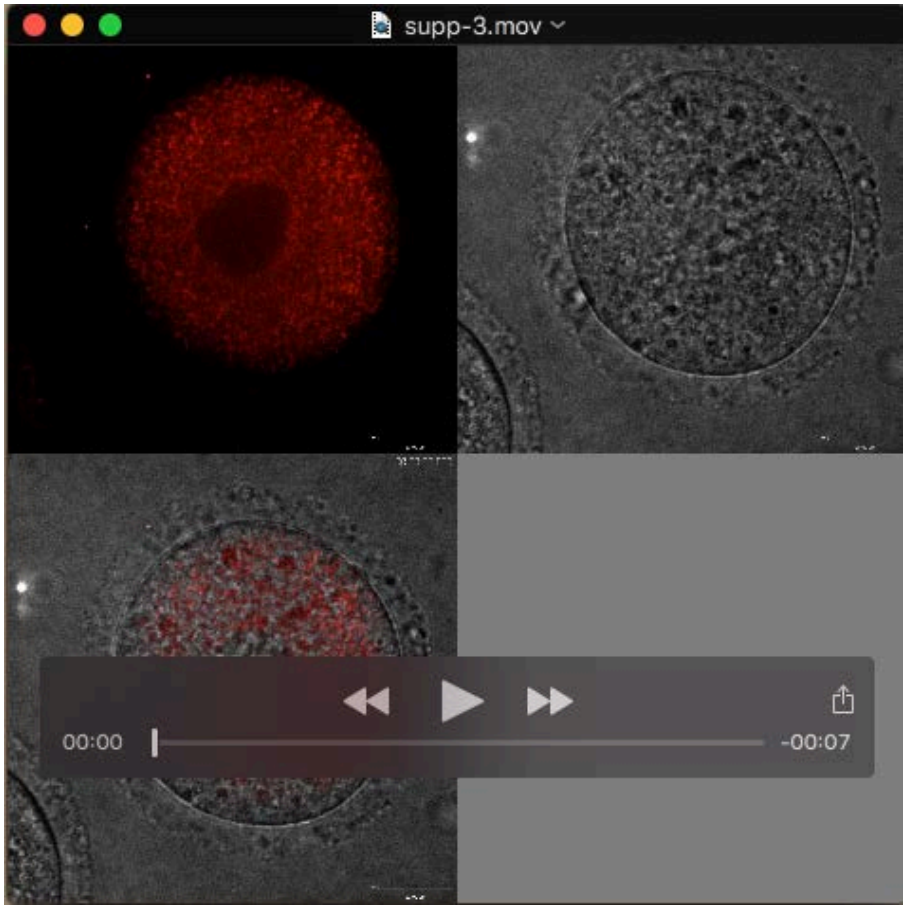

Movie 3. Mitochondria dynamics in the oocytes from *Nlrp4f*$^{+/+}$ females during GV to MII maturation. GV oocytes from *Nlrp4f*$^{+/+}$ females were labeled with MitoTracker for mitochondria and cultured to MII stage. Time-lapse images were captured every 30 mins with UltraVIEW-VoX. Related to Fig. 4D.

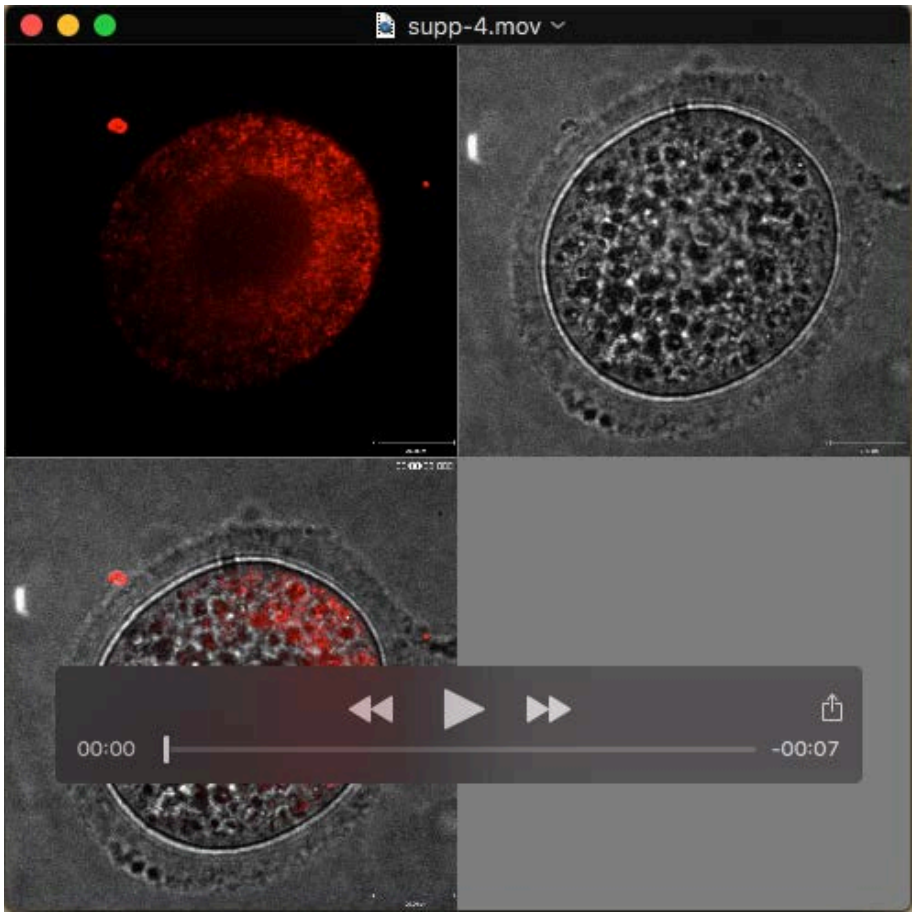

Movie 4. Mitochondria dynamics in the oocytes from *Nlrp4f*$^{-/-}$ females during GV to MII maturation. GV oocytes from *Nlrp4f*$^{-/-}$ females were labeled with MitoTracker for mitochondria and cultured to MII stage. Time-lapse images were captured every 30 mins with UltraVIEW-VoX. Related to Fig. 4D.